Please adjust group name in tumuser.sty.
Department of Electrical and Computer Engineering
Technical University of Munich

Compact CPA for Optical Inter-Satellite Communication Terminals on CubeSats

Leon Garidis

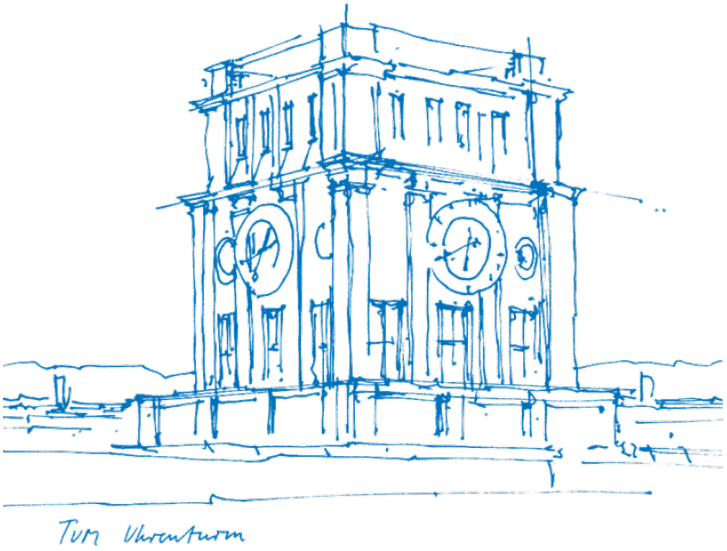

Please adjust group name in tumuser.sty.
Department of Electrical and Computer Engineering
Technical University of Munich

Compact CPA for Optical Inter-Satellite Communication Terminals on CubeSats

Leon Garidis

Thesis for the attainment of the academic degree

Master of Science (M.Sc.)

at the Department of Electrical and Computer Engineering of the Technical University of Munich.

Examiner:
Prof. Dr. Christoph Günther

Supervisor:
René Rüddenklau

Submitted:
Munich, 30.11.2022

I hereby declare that this thesis is entirely the result of my own work except where otherwise indicated. I have only used the resources given in the list of references.

Munich, 30.11.2022 Leon Garidis

Abstract

This paper explores an optical component of the communication link between CubeSats, which enables a laser data link between two satellites that are not aligned properly. The goal of this paper is to develop a stand-alone mirror system that can be attached to a preexisting communication terminal to increase its range of operation and enable satellites to form an uninterrupted communication network.

First, the technical requirements for the mirror system is defined based on existing low earth orbit (LEO) constellations. The space environment for LEO is identified and its challenges for electrical components summarized. With these technical and environmental requirements, multiple mirror systems are compared to find the best option for the application.

A test set-up was designed in order to be able to test mirror systems and characterize their behavior. All the components of the test set-up were tested separately, in order to minimize uncertainties in the actual mirror tests. The position sensitive device, which detects the mirror movements, was not suited for the required application. Therefore, future tests of different sensors have to be undertaken to find a good match. At the end, two options for the technical setup of a CubeSat Unit are explored and simulated.

Contents

List of Abbreviations

4QD	4-Quadrant Diode
AFOV	Angular Field of View
CA	Clear Aperture
CPA	Coarse Pointing Assembly
CubeSat	Cube Satellite
DLR	German Aerospace Center
FSM	Fast Steering Mirror
ISL	Inter-Satellite
LEO	Low Earth Orbit
LOS	Line of Sight
NMS	Newson Mirror System
PCB	Printed Circuit Board
PSD	Position Sensitive Detector
SMA	SubMiniature version A
SPI	Serial Peripheral Interface
TESAT	Tesat-Spacecom GmbH & Co. KG

1 Introduction

The number of satellites in low earth orbit (LEO) have been steadily increasing. Companies are trying to build 'mega constellations' of communication satellites to provide new kind of low-latency and high-throughput connectivity. These will cut down the latency from 250 - 300 milliseconds (in the case of geostationary satellites) to a few tens of milliseconds, enabling entirely new classes of exciting applications such as low-latency algorithmic trading across distances to difficult-to-reach locations such as oil rigs [30]. From 2019 to 2021, the number of active and inactive satellites in LEO has increased by over 50%, to over 5,000. SpaceX has plans for 11,000 more satellites for its Starlink network and has filed for an additional 30,000 with the with the Federal Communications Commission. OneWeb, TeleSat, and Amazon have plans to launch their own 'mega constellations' of communication satellites. [3].

The problem of providing a reliable connection between fast-moving objects in space is extremely complex and many aspects have yet been unsolved. The need for new network protocols and architecture research, in combination with space certified hardware create challenging hurdles [30]. This thesis investigates a solution for the challenge of laser communication between differently oriented satellites that are on the same orbit. While the satellite's payload is pointing towards earth, the inter-satellite communication terminals are not aligned. To safeguard connectivity, a coarse pointing assembly (CPA) redirects the laser beam towards the next satellite. Its goal is to compensate an angular offset between two satellites of $\leq 10°$. The approach, possible hardware components, testing and characterization of that hardware, and a final integration into a CubeSat in combination with an inter-satellite communication Terminals (ISL Terminal) are explored in depth in this thesis. In order to be able to carry out these tests, a test track was developed, which acts as a stable platform for testing procedures of the hardware for the compact CPA. The test track's design and functionality are also discussed in detail during this thesis.

1.1 CubeSats

The name *CubeSat* derives from the words *cube* and *satellite* . It reflects the size and shape of this type of satellite. The CubeSat project was started in 1999 between Prof. Bob Twiggs at Stanford University's Space Systems Development Laboratory and Prof. Jordi Puig-Suari at California Polytechnic State University (Cal Poly). The goal of the CubeSat project was to increase accessibility to space by reducing development time and cost, while sustaining frequent launches.

A CubeSat is a class of satellite that adopts a standard size and form factor, whose unit is defined as 'U'. A 1U CubeSat is a 10 cm cube with a mass of up to 2 kg. These singular units can be put together to form a satellite of up to 12U. The most common configurations are 1U, 1.5U, 2U, 3U, 6U, and 12U. How these configurations are put together is described in detail in [6]. A schematic of a CubeSat unit is shown in Figure 1.1.

CubeSat guidelines dictate the physical dimensions of a CubeSat, their secondary objective is to provide information on CubeSat dispensers and their corresponding interfaces. The goal is to implement good engineering practice, testing, and verification of systems. As a result, every engineer working on CubeSat satellites plays an active role in ensuring the success and safety of CubeSat missions.

Yet, the guidelines set forth in [6] are not enforced. The developer of a CubeSat must only meet the requirements given by the launch provider. The CubeSat Program's requirements are meant for preliminary design purposes only and provide sufficient freedom to comply with any launch vehicle.

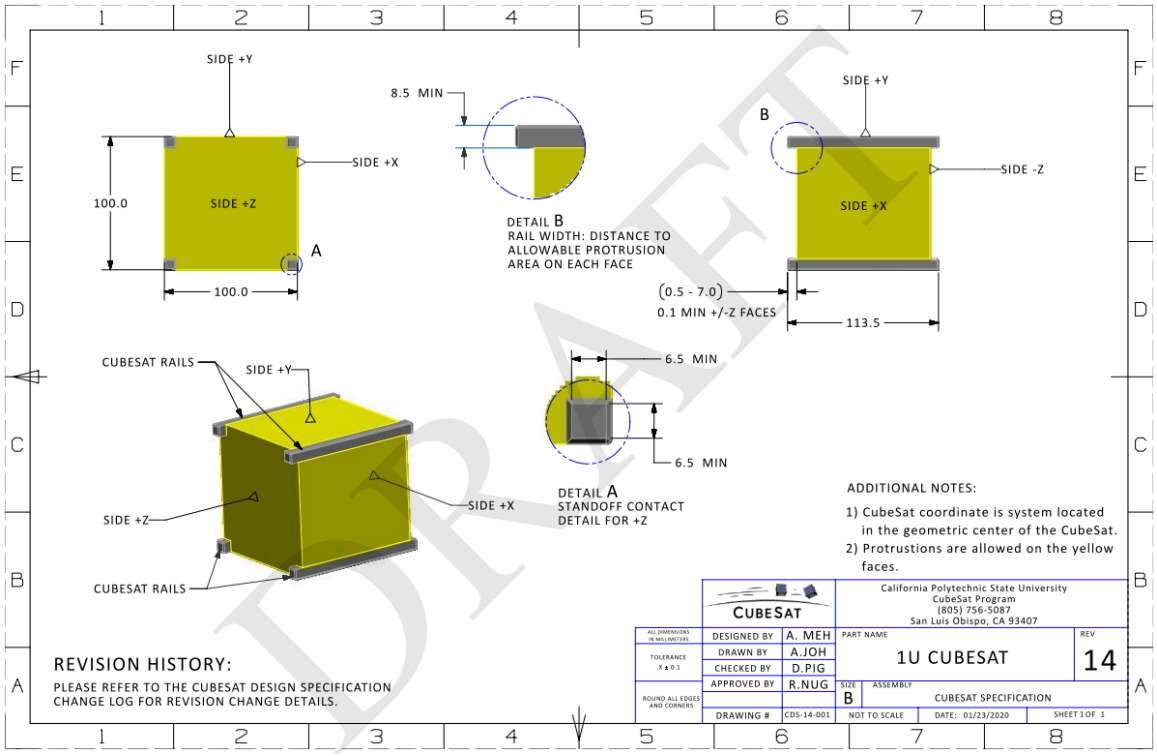

Figure 1.1 1U CubeSat Design Specification Rev.14 [6]

1.2 Motivation

Not only does the small size of a CubeSat limit the possible payloads that can be integrated into a satellite, but the small size also limits the power budget and the possibility of high power intensive operations. For communication and observation satellites, it is especially important that a satellite's payloads are always pointed towards the target area. Any further body pointing costs energy and, more importantly, can interrupt the satellite's mission. Inter-satellite communication enables the establishment of stable communication within satellite networks, without all satellites having to be connected to a ground station. Accordingly, it is of high importance to develop concepts that increase inter-satellite utilization and connectivity. A CPA is one of these concepts.

Laser communication between satellites allows very high data rates to be exchanged over long distances while consuming less energy compared to standard radio communications. This is due to the more targeted nature of laser communication in relation the dispersion of radio waves. However, its targeted nature also requires great accuracy when aligning communication satellites. The laser beams cannot be redirected through the communication terminal. Accordingly, the satellites must align themselves in order to be able to hit each other with their lasers. However, when two satellites align with each other, they cannot communicate with the next satellite in orbit because they can only align with one satellite at a time. This means that a continuous communication network between several satellites cannot be established.

A CPA uses motorized mirror actuators to redirect the laser beam from the communication terminal towards the next satellite. The movement range of the actuators define the angle a CPA can compensate. There already exist a large CPA that has $180°$ hemispherical coverage. However, due to its size and power draw, it is not always possible to integrate it into a CubeSat. Most communication links also do not require such large angular offsets compensations. As a result, this large CPA would not be the right system for most CubeSat applications.

This thesis examines the concept of a compact CPA. Its purpose is to be installed in the use cases, where the large $180°$ hemispherical CPA is over fitted. It is designed for the communication between satellites that are on the same orbital path. As a result, the required angular compensation decreases and the footprint of the CPA can be shrunk. With it, the required power draw and mass also decreases. As

a result, a system is developed, that is optimized for a specific window of angular offset compensation. Nevertheless, due to the planned orbital arrangement of mega constellations, this particular angle window will be applicable in many situations. Accordingly, the advantages that one gets from such a system are justified by the development effort. This thesis is the first step in the development of this compact CPA.

1.3 German Aerospace Center

The German Aerospace Center (Deutsches Zentrum für Luft- und Raumfahrt (DLR)) is the Federal Republic of Germany's research center for aeronautics and space. It conducts research and development activities in the fields of energy, transportation, security, aeronautics, space, and digitization. With over 10,000 employees at 30 locations in 5 countries, DLR serves as an umbrella organization for one of Germany's largest project management agencies [9].

Its space branch deals with research about topics ranging between earth observation, space exploration, communication, navigation, and quantum technologies. The communication institute concentrates its research and development on satellite-based processes and systems that enable widespread, comprehensive, independent and secure access to communications and navigation services [8]. In cooperation with the telecommunications company Tesat-Spacecom (TESAT), DLR has developed a communications terminal, known as OSIRIS4CubeSat, that enables data transmission up to 100 times faster than conventional radio links. Its biggest advantage to conventional systems is its size factor. With dimensions of just 10 x 10 x 3 cm, it fits perfectly onto small satellites. In combination with its minimal power draw, it is the first laser communication terminal that can be placed onto a CubeSat [10]. Through a combination of this terminal, named CubeLCT by TESAT, and the compact CPA from this thesis, it will become possible to establish effective inter satellite connections.

2 Optical System

The main component of the optical steering system is a motorized movable mirror. Its purpose is to deflect the outgoing and incoming laser beams in such a way, that they most effectively hit the other satellite or the communication terminal respectively. The communication terminal used in this thesis is the Inter-Satellite Terminal (ISL Terminal), and is pictured in Figure 2.1 and described in detail in [24]. It is a modified version of the CubeLCT Terminal designed for TESAT. It consists of three main components: the optical subsystem with the attached data receiver in the middle, the optical amplifier at the top, and the data handling unit at the bottom of the 1U ISL Terminal. The aperture of the telescope element on the ISL Terminal is 20 mm and has a compression ratio of $20mm/7.289$ [24]. The telescope is on the left side of the optical subsystem of the setup in Figure 2.1. Its 20 mm aperture needs to be completely radiated by the incoming laser beam to be able to establish a stable connection. This is the task of the compact CPA: ensuring the irradiation of the telescope during movements of the satellite. A fast steering mirror (FSM) inside the ISL Terminal redirects and controls the laser beam onto and within the sensors. The bi- directional data transmission between satellites is enabled through a transmission and receiving laser beam, which are separated by wavelength. Both wavelengths, 1536.6 nm and 1553.3 nm, are in the C-band and operate through the same terminal. As a result, only one ISL Terminal is needed to establish a bi- directional communication link between two satellites.

The motorized movable mirror for the compact CPA must meet certain requirements in order to perform the intended tasks. In this chapter, the requirements for such a mirror system are derived and described and multiple systems from five different companies are compared.

2.1 Requirements

2.1.1 Reflective Surface

The 20 mm aperture of the ISL Terminal needs to be completely irradiated by the befalling laser beam so that sufficient energy reaches the sensor system. Therefore, the mirror of the compact CPA needs to have a reflective surface of at least 20 mm. However, due to the angular offset of the CPA mirror to the laser beam axis, the actual redirected diameter of the beam is smaller than the diameter of the mirror. This is due to the relationship

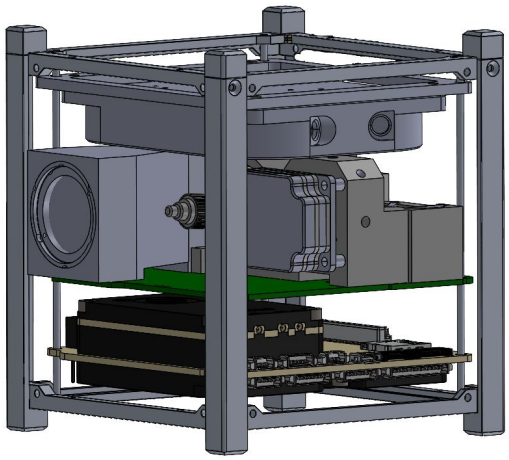

Figure 2.1 1U ISL Terminal [24]

$$d_{beam} = d_{mirror} * \sin(\theta). \tag{2.1}$$

As a result, the final reflective diameter needs to be larger than 20 mm. The larger the angle of incidence, the wider the diameter of the reflective surface needs to be. This is a dependent on how the mirror system is incorporated into the 1U CubeSat and how the laser beam is redirected to the aperture of the ISL Terminal. Therefore, the mirror diameter is required to be of at least 20 mm.

Another important aspect of the reflective surface is its surface quality, which impacts the amount of energy carried by the reflected beam. Flatness, has been proposed as a practical criterion for assessing the quality of an optical instrument by J. W. Strutt [14]. In the case where a beam reflects off a single mirror, the surface flatness will be equal to the wavefront distortion or the reflected wavefront error. Surface flatness typically is reported in units of fringes or waves and, as such, the surface flatness of a mirror is reported as a positive real fraction of the wavelength of light being used with the mirror [16]. The fraction λ/N, λ being the beam wavelength, represents the wavefront distortion and therefore describes the flatness of the surface. The larger N is, the flatter the surface is.

A noticeably distorted image occurs when the wavefront aberration exceeds $\lambda/4$ [14]. Therefore, the quality needs to be greater than $\lambda/4$. For their optics in communication systems, the DLR uses hardware that has a surface quality of $\lambda/10$. This ensures minimal wavefront distortions.

Coatings help decrease the loss of energy through reflection and further minimize distortion errors. The correct reflective coating for a specific wavelength needs to be chosen. The coating also needs to be able to withstand the harsh space environment, in order to retain its reflective properties. Since ISL Terminal operates in the infrared spectrum, the mirror coating needs to be able to reflect this type of wavelength well. Generally, silver and gold coatings are used in the infrared range. At the specific wavelength of 1540 nm, a gold coating has a greater percentage of reflectance of 98.9%, while a silver coating's percent of reflectance is 98.2% [7]. As a result, the mirror is specified with a gold coating.

2.1.2 Movement Range

The range of mirror movement is the most important technical value of the CPA. It defines the mission window, in which a CPA can compensate the angular offsets between communication terminals. The compact nature of the proposed CPA leads to a very restricted application window. It is defined by the limited space and opening of the CubeSat unit and the narrow mechanical movement range of the mirror system installed within the unit. The final angular offset is defined through the orbit data as well as the orientation of the satellite and the position of the communication partner.

To get an insight into the possible occurring angles, the mega constellations of the companies OneWeb, SpaceX Starlink, and TeleSat were examined. Plotting these constellations gives a sense of the challenge involved and the precision required to operate many consecutive satellites by linking them with laser beams. Figure 2.2 shows these constellations and their orbital planes.

Carizzo et al. [5] calculated the requirements for the beam pointing and beam slew rate of these three constellations, which are shown in Figure 2.3. All the calculations are based on a fully deployed network. The intra-plane links are established with the satellites directly in front and behind within the same orbital plane, while the inter-plane links are established with the satellites moving in the same direction in parallel orbital planes.

The topology of the OneWeb orbits requires beam pointing angles smaller than $-10°$ in elevation, and between $-50°$ and $+50°$ in azimuth. The maximum elevation angle to have a Line of Sight (LOS) between two satellites, before the curvature of the Earth comes in the way, is approximately $-30°$. Due to SpaceX's multiple orbital heights, the values differ slightly for each orbit. This can be seen in the multiple lines in Figure 2.3b. Overall, the required beam pointing angles have a maximum elevation range of $28°$, and $\pm 85°$ in azimuth. The maximum elevation angle to have a LOS between two satellites is approximately $-34°$. Due to the lower number of orbital planes and satellites per plane, Telesat requires beam pointing angles with a maximum elevation range of $48°$ and $\pm 80°$ in azimuth. Here as well, the maximum elevation angle to have a LOS between two satellites is approximately $-32°$.

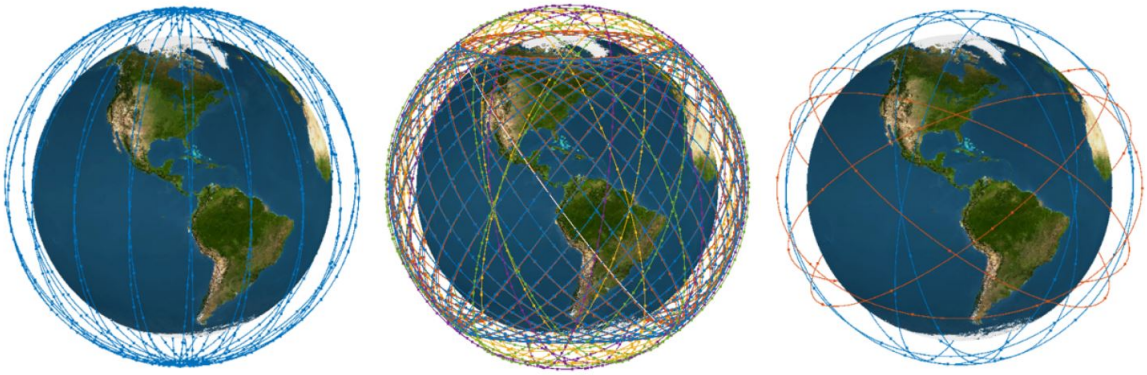

Figure 2.2 Satellite constellation of OneWeb (left), SpaceX Starlink (center), and Telesat (right) [5]

The DLR has already developed a CPA that moves in a hemispherical mode. So it can cover the large angles required for the inter-plane satellite links. The size constraints of the proposed compact CPA limit its use to the intra-plane communication links. As a result, the azimuth angles are about $0°$ and the elevation angles are in the low, single digit range. Telesat's elevation angles are an outlier due to their sparsely populated and higher orbits.

Through this comparison and discussions with manufacturers, the optical movement range requirement was set at $\geq \pm 4°$.

2.1.3 Speed

For the speed requirement, Carizzo and al. [5] calculations for the beam slew rate were used to get indications of the minimal required movement speeds of the mirror systems. These are shown in Figure 2.4. The values show the radial movement speed of the mirror movement necessary to keep up with the orbital change in orientation.

The slew rate needed in OneWeb's constellation is lower than $0.12°$ per second $[°/s]$ and is mainly defined by the azimuth beam pointing. Due to the different inclined orbits and their heights, SpaceX and Telesat have multiple lines in their graphs. The maximum values are being considered. SpaceX's maximum required beam pointing slew rate needed is $0.27°/s$ in azimuth and $0.03°/s$ in elevation. Lastly, Telesat requires a maximum beam pointing slew rate of $0.19°/s$ in azimuth and $0.07°/s$ in elevation. As discussed in the section above, the intra-plane values are mainly of interest. As a result, the required movement speeds of the mirrors are quite low.

A faster movement speed is preferred, however, as it relieves the system to not always operate at its maximum capabilities and it gives the possibility to use patterns to acquire communication links. As a

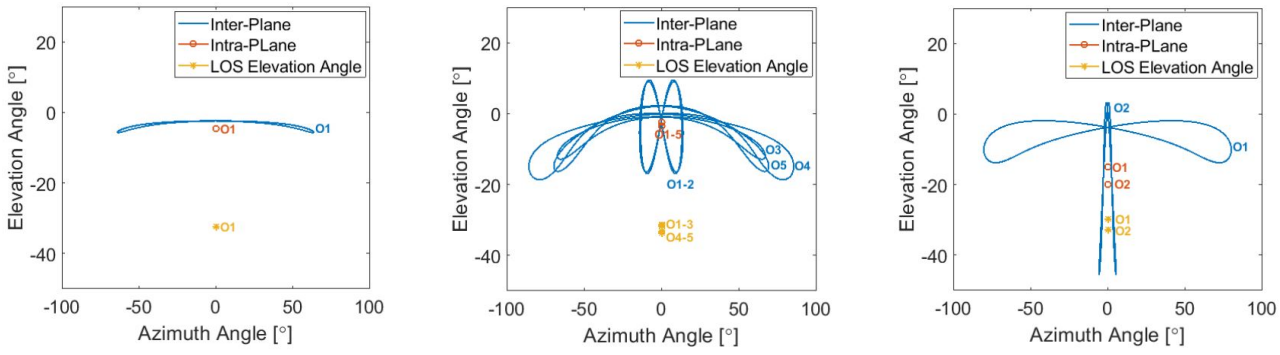

(a) OneWeb **(b)** SpaceX Starlink **(c)** Telesat

Figure 2.3 Requirements for beam pointing angles for OneWeb, SpaceX, and Telesat, based on calculations from [5]

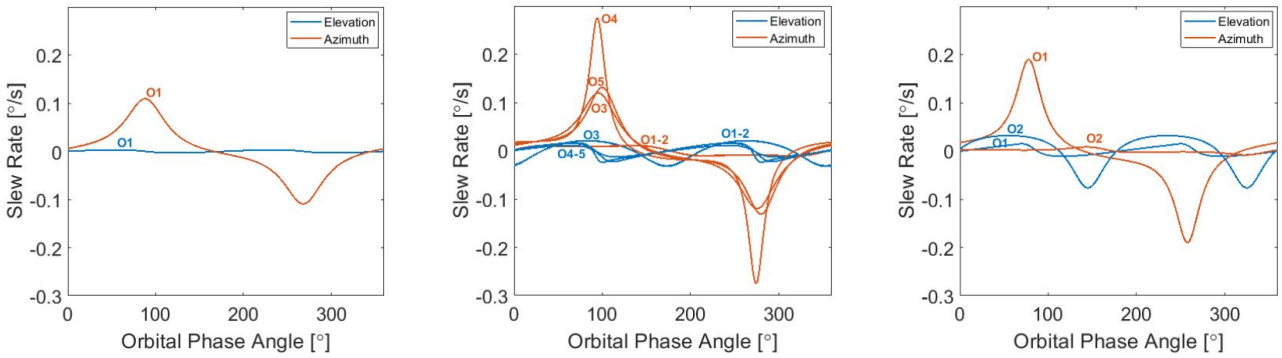

(a) OneWeb **(b)** SpaceX Starlink **(c)** Telesat

Figure 2.4 Requirements for beam slew rates for OneWeb, SpaceX, and Telesat, based on calculations from [5]

result, we believe that a final slew rate specification for the compact CPA of $\geq 0.1°/s$ is sufficient for the application.

2.1.4 Repeatability and Accuracy

The accuracy of the mirror system is of high importance. Due to the large distances between satellites, even a small angular divergences can lead to the communication partner not being engaged. The DLR has studied this subject and specifies components, that have an accuracy of $10\mu rad$. This was adopted to this mirror system.

The accuracy needs to be adequate enough, so that the FSM can first compensate for misalignment, but secondly also not overload the FSM. If the mirror's inaccuracy is too large but still within the movement range of the FSM, the FSM will not be able to perform its functions because its movement range will be exhausted to compensate for CPA errors.

2.1.5 Control Electronics

The size of a CubeSat limits the electronics in two main ways. First, the size constraint of the limited space available in a CubeSat requires that all electronics, including the power and control electronics, must be compact enough to fit into the 10 x 10 x 10 cm cube. In relation to the compact CPA, the mirror system and the control electronics need to fit into an 1U unit while still leaving enough space for the laser beam to be deflected correctly. An exact measurement of the maximal allowable size of the CPA electronics is difficult to estimate, since it depends on the selection of the final system and its positioning within the 1U unit. In any case, however, each axis needs obviously to be smaller than 10 cm.

Secondly, the power budget of a small CubeSat is very constrained. Generally, the larger CPA designed by DLR, which can move hemispherically, has a power draw of 60 W. Due to the smaller size and fewer moving components, the compact CPA's power draw should be below this value. The lower the power draw, the more often the compact CPA may adjust its offset to ensure a stable connection during transmission. Especially during transmission, when all of the laser, modulation electronics, and computing draw power, a considerable power demand from the CPA might not be supported. Therefore, the smaller the power draw of the compact CPA is, the more effective will the system become. The requirement is set at $\leq$ 60 W, since this level has worked successfully on a flight proven system, but a lower consumption is strived for.

2.1.6 Operational Environment

Space is a very harsh environment. Therefore, the space environment determines the design of a technical device more than almost any other environmental condition. The following list includes all challenges that components of a spacecraft have to withstand successfully for the entirety of their mission. They can be broken down into naturally occurring and induced challenges.

Naturally occurring challenges:

- Vacuum
- Micro-gravity
- Radiation
- Geomagnetic Fields
- Atmosphere

Induced challenges:

- Thermal Management
- Vibrations

All aspects of the operational environment are discussed in detail below.

Vacuum

Systems in space need to be able to operate in a vacuum. Space vacuum in the interstellar region is generally defined as an area of a ambient pressure of $\leq 10^{-15} Pa$. In LEO, however, the pressure increases to $10^{-7} Pa$ [17]. The absence of an atmosphere causes multiple problems. The main three are the following:

- Sublimation / Outgassing
- Change in material properties such as strength and service life/material fatigue
- Missing Convection

Due to the low ambient pressure, gas deposits and water vapor exhaust from the material lattice into space. As soon as the ambient pressure reaches or falls below the specific vapor pressure of the material, atoms or molecules from the surface evaporate. This process is called sublimation. The generic term for the escape of gases or particles from the surface of a material is called outgassing. The outgassing rate rises with the ambient temperature. As a result, materials experience mass loss and changes in their surface properties. The following materials are particularly prone to outgassing:

- Water
- Solvents
- Additives, e.g. plasticizers
- Traditional Lubricants

The outgassing products pose a risk to sensitive components, for example optical instruments, thermal coatings, high-voltage equipment. The outgassed materials can settle on the optical elements and reduce their efficiency or even impair their functionality. Traditional lubricants used on Earth are therefore not suitable for use in space, as they generally have a higher specific vapor pressure and their lubricating properties are often based on absorbed gases or water.

Strength, durability and fatigue of materials undergo changes in the high vacuum environment. Generally, the lifespan of mechanically stressed components increases. For many materials, the lifespan can increase by an entire order of magnitude [17].

In vacuum, the resistance to movement due to atmospheric pressure is non-existent. If the control loop of a mirror motor has been commissioned under atmospheric conditions it may lead to unpredicted movements in mirror behavior in space, due to the lack of dampening effects of the atmosphere. As a result, the mirror needs to be tested under vacuum.

Micro-gravity

The long-range nature of gravity means that the gravitational field generated by the Earth extends far into space. For example, at the height of the International Space Station, the Earth's gravitational pull is still about 90 % of its value on the Earth's surface. The phenomenon of apparent weightlessness of objects in orbit is of dynamic origin and has to do with the frame of reference from which the motion of other bodies is observed. In the framework of classical physics, the observer watching from the outside is in an inertial frame, the object, however, is in a reference frame accelerated to the inertial frame. Newton's laws of classical mechanics are valid only in an inertial frame. In order that the laws of mechanics are still valid in an accelerated frame of reference, we have to postulate an additional force which just cancels the acting gravity, so that our observation of the body at rest is in harmony with the freedom of forces following from Newton's axiom. This force is called apparent force F_s and is inversely proportional to the acceleration of the reference system relative to the inertial system. In the case of circular acceleration, the apparent force takes the form of a centrifugal force [17].

For a mass point m orbiting the Earth at distance R with angular velocity ω, the centrifugal force has the magnitude

$$F_c = m\omega^2 R \tag{2.2}$$

It must compensate the Earth's gravity, defined by

$$F_g = -\frac{\gamma M m}{R^2} \tag{2.3}$$

where γ is the gravitational constant and M the Earth's mass. In the equilibrium of both forces one obtains

$$\omega^2 R^3 = \gamma M = const \tag{2.4}$$

By considering the two equations 2.2 and 2.4, it becomes clear that weightlessness can only apply to one mass point. For an extended body, like a satellite, both forces compensate each other only along a line, which corresponds approximately to the trajectory of the center of gravity of the body. If one deviates from the center of gravity vertically to the flight path, the compensation is not complete. As a result, one experiences residual acceleration, also known as micro-gravity. At an altitude of 300 km, this residual acceleration is about $0.3 * 10^{-6} g_0 m^{-1}$ in the radial direction and $0.1 * 10^{-6} g_0 m^{-1}$ in the lateral direction, where g_0 is the value of gravitational acceleration on the surface of the Earth [17]. The chosen mirror system needs to be able to keep control of its deflection surfaces during these accelerations.

Under zero-gravity conditions, the effects of sedimentation, convection, and hydrostatic pressure disappear, leading to novel conditions, especially for studies of processes in which at least one fluid component occurs [17]. Since small mirror system do not use subsystems with fluids and do not require extensive cooling mechanisms, this study will not investigate this further.

Radiation

The Earth is subject to a nearly constant flux of charged particles and beta and gamma rays. Solar flares are the main origin of radiation flux, while omnidirectional cosmic radiation originated from outside the solar system is a second minor source. Especially in LEO, the cosmic radiation plays an insignificant role.

High-energy electrons and protons from solar winds are captured by the Earth's magnetic field and concentrate in radiation belts, also known as Van Allen belts. The inner radiation belt extends 200km from the Earth's surface because of the tilted and shifted Earth's magnetic field in relation to the Earth's axis of rotation. This so called South Atlantic Anomaly dominates the dose of energetic particles in low-inclination LEO [17].

These high-energy particles can cause damage to satellites through ionization, especially to electrical components. Such an ionization, which is often reversible at first, leads to the additional generation of charge carriers and causes a temporary failure of a component. Without the application of countermeasures, considerable irreversible consequential damage can be induced which can ultimately lead to the total failure of the component [17].

To protect systems against space radiation, one can either use radiation hardened components that can withstand the expected radiation or install extra shielding to absorb the high-energy particles. Extensive simulation and testing need to be undertaken to get a better understanding of the radiation environment expected during each mission. During testing, the parts are irradiated with ionized particles to find out at which ionizing dose levels the parts fail. This level summarizes the total absorbed energy by a component.

Geomagnetic Fields

In physical terms, magnetics represent a completely different natural phenomenon than gravitation. Internal magnetodynamic effects in a celestial body are primarily responsible for magnetic fields, not the existence of the celestial body itself. Furthermore, not all planets have a distinct magnetic field. Magnetic fields are neither spatially nor temporally constant, which poses an additional layer of complexity to inter-satellite communication [17].

In space travel and spacecraft design, the movement of a spacecraft in a magnetic field causes an induced electric voltage in electrical components. This can lead to localized electrical potentials in a spacecraft of the magnitude of several volts. Additionally, the formation of radiation belts and the acceleration of charged particles toward the magnetic poles of Earth cause certain spacecraft orbits to be exposed to increased radiation.

The magnetic fields can also influence other components than just the electronics. Systems using coil mechanisms for movable parts can be influenced in their accuracy.The applied magnetic force by the coil to move specific components can be disturbed by outside forces, leading to false adjustments. This phenomenon must be tested before a system can be installed into a spacecraft.

Atmosphere

The impact of the atmosphere on satellites is only applicable in low LEO. The heterosphere is a part of the atmosphere that extends from an altitude of 100 km to approximately 400-500 km. Here, the individual neutral gas components are distributed in the Earth's gravitational field in such a way that the percentage of lighter gases increase as the distance from Earth increases. Due to the marginal density of the lighter gases, some can achieve velocities that are above the escape velocity and can escape into interplanetary space, where the exosphere starts [17].

Over time, these particles can slow down satellites through friction. To keep the satellites in orbit, their course must be corrected. Since the compact CPA does not control the movement of the satellite, the gas particle induced friction is out of scope for this thesis.

Vibrations

Vibrations occur during all phases of a space mission; they are strongest during liftoff and during transit into space, but routinely occur also during the course of the mission or during altitude control maneuvers and separation operations. The occurring frequencies cover a range from 1 to 2000 Hz and can be categorized into two groups. The low frequency range of 1 to 100 Hz are transient or quasi-harmonic vibrations and the high frequency range of 20 to 2000 Hz are randomly distributed, noise-like vibrations [17].

The biggest problem resulting from vibrations is the resonance behavior of a satellite section. This describes the oscillation of a system at its natural or unforced resonance. Resonance occurs, when the energy in a system can be stored and is easily transferred between various storage modes such as kinetic and potential energy. Most systems have a resonant frequency and several harmonic frequencies whose amplitude decreases with increasing distance from the geometrical center.

If the resonant frequencies of the CPA match the frequencies occurring in the CubeSat, the oscillations would build up and could lead to interference behavior or even mechanical failures.

Dynamic mechanical loads can be simulated with vibrational tests. Below are two types of excitation that can be used for testing

- Sinusoidal Excitation
- Noisy Excitation (random).

In order to test these dynamic mechanical loads, a system is mounted on a rigid vibration table through which the vibration excitation is transmitted. The qualifications for components are the ISO_9022-3-36-04-1 for sinusoidal excitation and ISO_9022-3-37-11-1 for random vibrations. Components that have passed these tests are suitable for space applications [17].

A harsh and short vibration is a shock. This type of mechanical stress is characterized by high acceleration –up to 100 000 m/s^2– with a very short duration of action of 10 to 20 ms and is thus less relevant for main structures than for electronic, precision mechanical and optical components [17]. Shocks originate from short-term shock-like mechanical loads. These are generated during launch of a rocket by the ignition of propulsion systems and mainly by pyrotechnic activation of release mechanisms. The chosen mirror system needs to withstand the occurring shock vibrations during launch and separation to ensure its full functionality once in orbit.

Thermal Environment

The thermal operating environment of components in space play an important role in the design. To safeguard the components' functionality, they need to be kept within their designed thermal operation range. The produced heat output needs to be transferred to its environment. On Earth, three processes of heat transfer exist.

- Conduction: the transfer of heat through objects that are in physical contact.
- Radiation: the transfer of energy by the emission of electromagnetic radiation.
- Convection: the transfer of energy between an object and its environment due to fluid motion.

Due to the vacuum in space, the use of convection is not possible. Thus, a satellite can interact with its thermal environment only through radiation. The size and power budget constraints of a CubeSat, make it impossible to integrate a powerful cooling system using convection heat transfer. Therefore, the heat output of the electronics must be emitted by radiation from the outer surfaces of the 1U enclosure. The background temperature of space is $T_b = 2.7K$, creating a large temperature difference between space and the CubeSat's electronics [17]. It is not possible to add more radiators to increase cooling capacity, as they would violate the defined size of a CubeSat unit.

In addition to the thermal energy produced by the electronics and components, the CubeSat absorbs thermal energy from its environment. There are two main factors that influence the thermal environment in LEO. One is the direct radiation of the sun. Planck's radiation law of a cavity radiator approximately describes the solar spectrum, ranging from the near UV to the visible and infrared range. The energy flux density integrated over all wavelengths at 1 AU distance from the sun is called the solar constant. AU is the average distance from Earth to the sun and is called an astronomical unit; 1 AU is equal to $1,496 * 10^8 km$ [17].

The second environmental thermal energy that influences the temperature of the CubeSat is the solar radiation reflected back from the Earth as well as the infrared radiation emitted by the Earth as a warm body. The solar radiation reflected from a planet and its incident on a satellite is called Albedo. The Earth's Albedo amounts to 30 % of solar radiation. Because of the thermal capacity of the external satellite materials, the Albedo variations usually do not have a large effect on the satellite temperature. The effects are most likely to affect the outer layer of the satellite's low-capacitance insulation, but the effect is not critical there. The effects of the Albedo radiation on the satellite decreases sharply as orbit altitude increases. The radiation emitted by the Earth is in the infrared range and corresponds to a black-body temperature of about 250 K. The average radiation energy is in the infrared range and in LEO averages around 230 W/m^2.

The vast majority of today's space systems operate in the conventional temperature range between about $-40℃$ and $+50℃$ for components mounted inside the satellite. For external equipment, much wider ranges of $-170℃$ to $+120℃$ usually apply [17]. These ranges generally protect the system from the adverse effects of thermal energy. There is a scenario, however, in which sunlight can enter the open front of the compact CPA unit and hit the internal components directly, causing them to heat up more rapidly. This use case needs to be explored further, to make sure that all components can function during direct radiation from the sun. The thermal modeling for this use-case is outside the bounds of this thesis.

2.1.7 Final Requirements

Based on the above analysis all finalized specifications for the mirror assembly are listed below:

- Mirror diameter: $\geq 20mm$
- Movement range: $\geq \pm 4°$
- Accuracy: $\leq 10\mu m$
- Speed: $\geq 0.1°/s$
- Power consumption: $\leq 60W$
- Compact electronics
- Space environment compatible

2.2 Possible Partners

An in-depth online research concluded that only a limited number of qualified vendors offer mirror systems that meet the requirements mentioned above. We explored further options at the Laser World of Photonics trade fair in Munich, Germany on April 26th till 29th, 2022.

At the trade fair, the team pitched the mirror system requirements were pitched to multiple companies. While many did not have a product that could match the requirements, some proposed workable options. All eligible systems, their advantages and disadvantages are described in the following sections.

2.2.1 THORLABS

THORLABS, an American company based in Newton NJ, has two product classes, which could be an option for this project. One is their new FSM system and the other consists of a pair of galvanometers, that create two axis movement.

Fast Steering Mirror System

Thorlabs' FSM3 Fast Steering Mirror offers a high precision, closed-loop solution for single and multi-axis optical applications. It incorporates four voice coils into a compact flexure bearing support frame for fast and stable positioning of the mirror. Accurate and repeatable positioning is provided by an internal continuous position sensitive photodetector.

The main specifications of the FSM are listed in Table 2.1, while the system is shown in Figure 2.5a.

Mirror Diameter	Movement Range	Accuracy	Dimensions (LxWxH)
76 mm	$\pm 6°$	5 mrad	76 x 51 x 81 mm

Table 2.1 THORLABS FSM specifications

The biggest issue of the FSM is the size of its electronics in relation to a CubeSat Unit. The power supply unit's dimensions are 185 x 51 x 195 mm and the controller's dimensions are 199.2 x 105.2 x 323.8 mm. These dimensions totally exceed the volume constraints of a CubeSat. From a business perspective, it would not be economically feasible for THORLABS to reduce the size for these components due to the non-recurring engineering costs in the face of the very low number of units required for prototyping.

No further technical diligence was conducted, as the system's dimensions rendered it unsuitable for the CubeSat application.

Galvanometers

The second THORLABS solution is a system of two galvanometers. Each one would deflect the incoming laser beam on one axis. Two separate line of galvanometers came into consideration.

The specifications of the first galvanometer option, the QS line, can be seen in Table 2.2. While the diameter, movement range, and movement accuracy are within the specifications, each galvanometer is too long to fit into a CubeSat unit. Since two would need to be mounted perpendicular to one another to achieve the two axes deflection, as seen in Figure 2.5b, the system would exceed the dimension limits in two directions, as seen in the dimensions tab of Table 2.2. The QS line deploys bearings, which require lubricants. This poses a problem as these lubricants are not rated for use in a vacuum. Again, an extensive redesign of the bearings would not be feasible for THORLABS for the required quantities. Therefore, these galvanometers are not suitable for the CPA.

Mirror Diameter	Movement Range	Accuracy	Dimensions (LxWxH)
$\leq$ 45 mm	$\pm 22.5°$	15 μrad	153 x 100 x 127 mm

Table 2.2 THORLABS QS line galvanometers specifications

The SS30 and SP30 flexure galvanometers were the second option. They do not use bearings due to their use of moving magnets. These moving magnet galvanometers are ideal for raster imaging applications, feedback-stabilized imaging systems, or as tracking scanners for viewing or marking moving objects but wear out quickly when used for step-and-settle motions. Their biggest constraint is the size of the servo amplifier, which is 60.5 x 54.1 x 27.0 mm. The two required amplifiers would not fit into a CubeSat unit. Additionally, the unsuitable operational mode render the flexure galvanometers not suitable for this project. Therefore, THORLABS does not offer a system which can be used in this compact CPA.

2.2.2 SmarAct

SmarAct is a German company that specializes in high-precision positioning, automation, and metrology. SmarAct produces a gimbal type mirror mount, the AmarAct STT-2013-Tip-Tilt-Mirror Mount, that offers a wide agular travel range. The gimbal system is depicted in Figure 2.5c. The two motorized stages move independently from each other, leading to great flexibility. The design is vacuum compatible and can operate in a large temperature range. Its compact design fits into the CubeSat unit and the control circuit board can be designed compactly as well. The main specifications are listed in the table below.

Mirror Diameter	Movement Range		Accuracy	Dimensions (LxWxH)
25.4 mm	Axis 1: $\pm 90°$	Axis 2: $360°$	$\leq$ 10 mrad	35 x 46 x 61 mm

Table 2.3 SmarAct Gimbal specifications

SmarAct's gimbal system meets most technical requirements for this project, though some details like lubricants would need to be further discussed with the designers. Yet, the delivery time of 30 weeks exceeds the time frame of this project. In addition, further design conversations and implementation time will be needed. Therefore, the AmarAct STT-2013-Tip-Tilt-Mirror Mount was not chosen for this thesis.

2.2.3 MRC System GmbH

Another possible partner is MRC Systems GmbH. This German company specializes in innovative medical, electronic and laser optical products. They offer a wide variety of compact actuators for laser beam stabilization. Their flagship system, the P4S30-Piezo tilting mirror, is able to provide high accuracy and

speed. However, its mechanical movement range is very limited and not sufficient for this project. The actuator is shown in Figure 2.5d.

Mirror Diameter	Movement Range	Accuracy	Dimensions (LxWxH)
2.5; 3.8; 5.08 mm	$\pm 0.23°$	2 μrad	67.5 x 50 x 63 mm

Table 2.4 MRC Systems P4S30-Piezo tilting mirror specifications

The company's spokesperson mentioned however, that the company is working on a prototype with a larger movement range. There, three screws will be used to move the vertical plate, which holds the actuator, using small step motors. This could satisfy the required movement range. The development of the prototype was, at the time of the fair, still in early stages. This concept has several points that still need to be developed for space applications like the required lubrication for the screws, the high number of moving parts and their maintenance need. In addition, the large electronics control unit and a non-binding time frame for the completion of the prototype resulted in MRC Systems GmbH not being selected as a project partner.

The company's spokesperson mentioned that the company is working on a prototype with a larger movement range. This prototype includes three screws that will move the vertical plate, which holds the actuator, using small step motors. This could satisfy the required movement range. At the time of the fair, the development of the prototype was still in its early stages. This concept has several points that still need to be developed for space applications like the required lubrication for the screws, the high number of moving parts, and their maintenance need. In addition, MRC Systems GmbH was not selected as a project partner due to the large electronics control unit and a non-binding time frame for the completion of the prototype. .

2.2.4 Newson

The last possible partner is the Belgian company Newson that specializes in high precision measuring and control engineering. Their patented *rhothor* technology brings benefits of moving coil technology to their actuators. This technology allows to control larger apertures with lower power consumption and low angular drifts. Their new Cyclops actuator is a single mirror dual axis system that has a greatly reduced size in comparison to the above mentioned options. Its basic characteristics are listed in the table below.

Mirror Diameter	Movement Range	Accuracy	Dimensions (DxL)
38.1 mm	$\pm 13.5°$	10 μrad	⌀60 x 46.5 mm

Table 2.5 Newson Cyclops specifications

This actuator system satisfied almost all requirements and was therefore chosen for this project. An in- depth view of the Cyclops system is conducted in the next section.

(a) THORLABS FSM System [26]

(b) THORLABS Galvanometers [27]

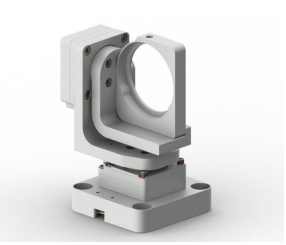

(c) SmarAct Gimbal System [25]

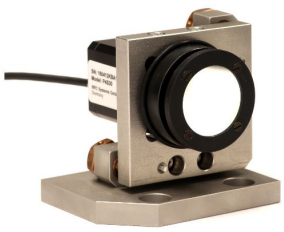

(d) MRC System P4S30-Piezo tilting mirror [12]

Figure 2.5 Various insufficient mirror system options

2.3 Newson Mirror System

All information can be found in the official Newson manual [18]. The Newson Mirror System (NMS) is depicted in Figure 2.6. Below we will concentrate on the relevant information.

2.3.1 Physical Characteristics

The physical characteristics of this system were decisive in its selection for this thesis. The most crucial feature is the mirror, which has a diameter of 38.1 mm. This satisfies the requirement of a $\geq$ 20 mm mirror diameter, while providing enough margin to keep the laser beam firmly targeted on the ISL telescope during movements. The correct mirror selection for the NMS is discussed further in 2.3.5.

The dimensions of the NMS are very favorable to the CubeSat. All its mechanical and electrical components are enclosed in a very compact casing. Its cylindrical shape of $\varnothing$60 mm x 46.7 mm is small enough to fit into a 1U CubeSat and be position freely. The complete technical drawing of the NMS can be seen in Appendix A.1. The size of its control electronics, further discussed in 2.3.3, and degrees of freedom for customization make the NMS especially effective for integration into the CubeSat.

The movement range of $\pm 13.5°$ in combination with its large diameter fully satisfies the movement criteria. As a result of the design of the coil mechanism, no part of the mirror is obstructed throughout the entire movement range, yielding full usage of the mirror diameter at all times. This is a unique advantage in comparison to other systems, where the reflected beam would get clipped at maximum deflections.

Furthermore, the accuracy does not suffer due to the large movement range. The NMS achieves a repeatability of 10 μrad, while the drift over 8 hours also stays minimal at 10 μrad. This minimizes communication errors due to inaccurate beam alignment and reduces readjustments due to drifts. Even in these conditions, the movement speed still satisfies the requirement. The entire $\pm 13.5°$ movement range can be traversed in 28 msec. For the step-and-settle motions of a CPA, these speeds will satisfy any future requirements.

2.3.2 Control Protocol

The NMS uses a 20-bit two's complement presentation for set point and actual position. For ease of use, the deflector has both a 20 bit and a 16-bit interface to exchange these values. The latter disregards the 4 least significant bits and only accesses the 16 most significant bits. A half-duplex Universal Asynchronous Receiver Transmitter (UART) connection is used to exchange the instructions and their response. The transmission of single byte takes 1.1 µsec. After reception, the deflector will process the data and start its response within 1.5 µsec. To avoid data collision, the time between different instructions must be at least 5 µsec for single byte and 10 µsec for multiple byte instructions. The difference between the 20-bit and 16-bit communication is listed in the table below.

Control	Resolution	Size Instruction	Size Reply	Execution Time
20-bit absolute set point	1048576 bits	3 bytes	3 bytes	10 µsec
16-bit relative set point	65536 bits	1 byte	1 byte	5 µsec

Table 2.6 Instruction overview of the NMS

The 20-bit communication is used in the scope of this thesis, therefore it will be examined further.

20-bit Absolute Set Point Control

While both axis receive set points and return actual position data, Channel 1 is padded with error flags. These can be used to fully monitor the operation of the deflector's operation.

When the distance between target and set point is too large, the target position is clipped following a maximum speed principle. The maximum speed whereby the set point is allowed to change, is set at 105

Mbit/sec. The error bit Err_POS is set to ONE, when clipping occurs. When this bit is cleared, no clipping occurred and the set point is loaded with the target position.

The deflector's consumed energy is dependent on the applied target position variations. It uses a dual stage protection system to protect itself from thermal damage. The first stage consists of a reduction in the set point speed. This occurs when the consumed power by the NMS is above the maximum load of 18 W. Then the error bit ERR_OVLD is set to HIGH. In case the power level rises above twice the maximum load, the second stage protection switches off the amplifier and the regulator. The deflector stops tracking and sets error bit ERR_TRACK. After 4 seconds the deflector reboots and the error is cleared. These three error bites, seen in the 4th row of Table 2.7, are only transmitted through the first channel.

Instruction Byte 1	START,0,0,0,0,S0,S1,S2,S3,0,STOP
Instruction Byte 2	START,S4,S5,S6,S7,S8,S9,S10,S11,0,STOP
Instruction Byte 3	START,S12,S13,S14,S15,S16,S17,S18,S19,1,STOP
Reply Byte 1	START,ERR_POS,ERR_TRACK,ERR_OVLD,0,A0,A1,A2,A3,0,STOP
Reply Byte 2	START,A4,A5,A6,A7,A8,A9,A10,A11,0,STOP
Reply Byte 3	START,A12,A13,A14,A15,A16,A17,A18,A19,0,STOP

Table 2.7 Serial Bit Sequence of the 20-bit communication protocol of the NMS

2.3.3 Electronics

The NMS is a very efficient system. Its average power draw is around 3 W, while it can peak shortly at 18 W. This is below the maximum power budget for the ISL Terminal. Due to the low average power draw, it is possible to continuously adjust the mirror and unload the FSM within the ISL Terminal. This then leads to a more stable connection and better data throughput.

The two movement axes are being supplied by two separate power supply lines. One SMA connector, per axis, on the back of the NMS acts as a power and communication port. The setpoints and actual deflector positions are modulated onto the power supply for each axis. This is done through an external printed circuit board (PCB) and its schematic is provided by Newson [18]. The data towards the deflector (TXD) is high pass filtered while the power supply is low pass filtered. The returned data is obtained by demodulation using a Schmitt trigger. Its output is the RXD.

The modulation electronics for one axis fit onto a 50 x 50 mm PCB. These can be stacked to have an electronic control unit with the dimensions of 50 x 50 x 23 mm for one NMS. This compact size makes it possible to fit it into one CubeSat unit. How the PCB was implemented is described in 3.4 and Figure 3.13a shows the final PCB layout. The PCB needs to be made out of radiation hardened components. Once put together, it must pass radiation testing to make sure its functionality is maintained during its lifespan.

Newson also provides a master control unit for all its actuators. It has the same functionality as the modulation electronics, but provides more connectivity and is built by Newson; as a result its functionality is guaranteed. This device was ordered as well as part of the CPA, The idea being that the NMS could be characterized using Newson built hardware and then the custom-build modulation electronics be tested. As a result, the functionality of these electronics be tested. It also simplifies the first interactions with the NMS.

2.3.4 Environmental Aspects

The NMS is not space certified. Due to its coil technology, it does not use any lubricants that would be problematic in space. Newson has not tested its resistance to shocks, vibration or radiation. Its thermal envelope in vacuum is not documented either. These properties need to be tested rigorously before the NMS can be deployed into space.

Figure 2.6 Newson Mirror System with a silver coated mirror [19]

2.3.5 Mirror

One of the main advantages of the NMS is its 38 mm diameter mirror. It is large enough to cover the use case for this application and offers margin for alignment error. The preferred thickness of the mirror is 2 mm, for which the coils are tuned. Newson sells the NMS with a silver coated mirror, which is optimized for 1064 nm wavelengths. However, the laser wavelength used in the ISL Terminal and in this thesis is 1540 nm. Therefore, the NMS was ordered without the mirror and a gold plated mirror of the same geometrical specifications was ordered separately.

No off-the-shelf mirror exists, which has a diameter of 38 mm and a 2 mm thickness and is optimized for the 1540 nm spectrum. As a result, a custom-made mirror had to be ordered. Several manufacturers could meet the mirror's surface quality and reflective specifications. Therefore, the production and delivery time of the mirrors became the critical path for this thesis. Because all manufacturers quoted lead times with delivery of the mirrors after the proposed end of this thesis and in order to still set up a testable system, a 3 mm thick, off-the-shelf mirror from Edmund Optics was purchased. The performance of the NMS is likely expected to suffer a little herewith, due to the extra weight of the mirror. Yet, the system can still be used and tested to provide valuable information. An additional 2 mm thick mirror from the company Laseroptik was ordered. The DLR wishes to continue using/developing the NMS after this thesis and will replace the 3 mm mirror with the originally specified one, when it becomes available. This thesis' characterization of the NMS with the thicker mirror is still valuable for the DLR, since it provides the base performance characteristics and operational behavior. The thinner mirror will certainly improve its performance but since the CPA does not have to move at high speed, it is understood that the performance of the thicker mirror will suffice for this use case.

2.3.6 Delivery Times

Newson was the only company at the fair, which promised a lead time of less than six months. The official delivery time quoted was 12 to 14 weeks. This relatively short delivery time was the deciding factor in choosing Newson as the project's partner. At the time, it was the only option that could deliver a mirror system within the time frame of this thesis. Please, note that the mirror itself was ordered separately, as described in the Section above.

However, the delivery date was postponed three times, with the lead time being extended to first 22 weeks and at the end to over 7 months, or 28 weeks. According to the manufacturer, the global supply chain disruptions that have affected industry this year have been the reason for the delays in the delivery of sub-components from sub-suppliers, such as chips and general electrical supplies.

Even with the delays, Newson still has the quickest delivery time of all suppliers. Ultimately however, the NMS was not delivered during the time frame of this thesis and therefore the timeline and scope of this thesis had to be adjusted. As a result, the NMS could not be characterized and the environmental impacts evaluated. The NMS remains the preferred optical component for the compact CPA, as all its technical advantages are retained. In order to simplify its future commissioning, detailed guidance for characterization and environmental testing is provided in Chapter 4. This will greatly simplify future work. The compact CPA will be further developed with the NMS and the preliminary designs are explained in Chapter 5. We hope that when the equipment becomes available, the original scope of this thesis can be completed.

2.4 Optotune Mirror System

Due to the final delivery time of the NMS and the time constraints of this thesis, it was decided to use an already available mirror system, which is being tested by the DLR for an intermediate coarse pointing assembly. The system is the *MR-15-30* fast steering mirror from the Swiss company Optotune. This mirror system was used to

The goals remained the same, but instead of developing the compact CPA, the focus was shifted to the intermediate CPA.

2.4.1 Physical Characteristics

The MR-15-30 is based on the voice-coil technology. This enables it to move a mirror across a large range of motion with very fast speeds.

Mirror Diameter	Movement Range	Accuracy	Dimensions (DxL)
15 mm	$\pm 25°$	40 μrad	$\varnothing$30 x 14.5 mm

Table 2.8 Optotune's MR-15-30 mirror system specification [20]

The very compact design of the MR-15-30 makes it extremely easy to implement it into a 1U CubeSat. The four mounting points ensure a firm connection. Due to its compact size, the mirror's diameter is only 15 mm, which is the main drawback in comparison with the originally selected Newson set-up. The usable diameter is reduced due to the suspension mechanism at large deflection angles. This is explained in more detail below; the mirror system is shown in Figure 2.8.

The mirror is suspended an a 2-axis gimbal system. This enables the mirror to have an angular movement range of $\pm 25°$, which satisfies the technical requirements. The repeatability is constant throughout the entire range at 40 µrad. No information about angular drift has been provided.

The coil technology also makes fast mirror adjustments possible. 20° steps can be completed in 13 ms. As a result, the entire movement range can be traversed in only 32.5 ms. Small angle step (0.1°) settling time is just 3 ms. For the step-and-settle motions of a CPA, these speeds will satisfy any future requirements.

Optical Clipping

Due to the large movement range in combination with the suspension mechanism, it is possible that parts of the reflected beam are being clipped, as shown in Figure 2.7. This results in the reduction of the usable mirror diameter with larger deflection angles. Therefore, the full range of motion can only be used, if the mirror is used in conjunction with a thin laser beam. Table 2.9 shows the percent of a 15 mm wide laser beam being clipped at an angle of incidence of $45°$, as well as, the possible laser beam diameters at a given deflection with no clipping occurring.

As a result, the full range of motion cannot be used in satellite communication. A clipped laser beam does not transfer enough energy to make communication possible.

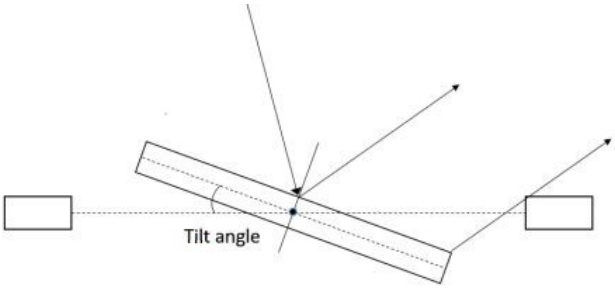

Figure 2.7 Optical clipping of the laser beam on the suspension mechanism [20]

Angular Deflection	$0°$	$\pm 5°$	$\pm 10°$	$\pm 15°$	$\pm 20°$	$\pm 25°$
Percent of $\varnothing 15mm$ clipped	0	14	24	34	44	54
Possible Laser Beam Diameter without clipping (mm)	15	10.9	7.9	4.8	1.7	N/A

Table 2.9 MR-15-30 laser beam clipping behavior [1]

2.4.2 Control Protocol

Optotune provides multiple ways to control the MR-15-30. A development kit is included in the scope of delivery. In standard form, it comes with a control electronics box that is connected between the computer and the mirror. It supplies the mirror with power and acts as an interface. With it, the mirror can be controlled though the *Optotune Cockpit* software. This software provides basic control and data visualization of the mirror functions. The full set of functions of Optotune Cockpit are explained in [21].

For this limited space application the mirror can also be controlled through a Serial Peripheral Interface (SPI), which can be used instead of the control electronics box rendering the system more compact and customizable. It uses the SPI Mode 1. The Interface accepts data on the positive edge of the clock and samples the data at the negative edge. Each transfer comprises of 14 bytes with 8 bits each. The 14 bytes are divided into 7 words with 16 bits each. The user can read/write data from and to the mirror. An example code for a write request is shown in Table 2.10. A full list of all commands can be found in [21].

Word	Description
0	Write flag (0x0001)
1	'System ID1' + 'Register ID1' to perform write
2	'System ID2' + 'Register ID2' to perform write
3-4	Data to write in address 'System ID1' + 'Register ID1'
5-6	Data to write in address 'System ID2' + 'Register ID2'

Table 2.10 Write command to MR-15-30

2.4.3 Electronics

The MR-15-30 operates at 15 V. While the mean actuation power is 1.5 W, the peak power draw can reach 30 W for 10 ms. The maximum power draw is below the maximum allowed power draw. Yet, this value only gets reached, if both axes move to their utmost deflection.

The electronics that control the mirror are mostly contained within the housing. As a result, no extra hardware is needed to control it. When using the SPI Interface to communicate with the mirror, the communication works at 3.3 V. The development kit comes with its own power supply that plugs into a typical outlet. Due to its size, the development kit is purely used during testing and cannot be integrated into the final product.

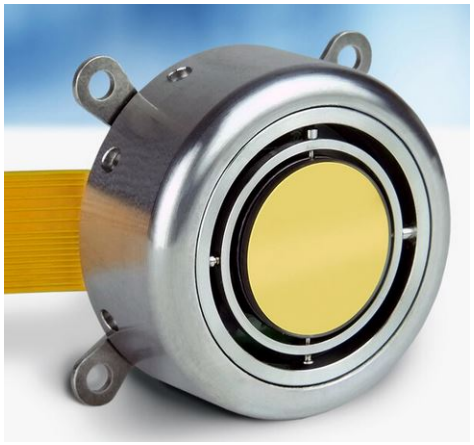

Figure 2.8 Optotune MR-15-30 [20]

2.4.4 Environmental Aspects

The MR-15-30 is not space certified. While it can withstand temperature swings from -20℃ till 90℃, shocks of 105g, and vibrations of 2g with a resonance of 10 - 150 Hz, it is not designed for the use in a vacuum. The joints use grease, which is not vacuum compatible. It would lead to outgasing, controllability issues, and eventually to the parts failure. A change of the lubricant will not be possible without a significant number of tests from the manufacturer.

Another aspect is the systems thermal envelope. it has not been tested to dissipate the power loss purely through radiation. The mirror withstands approximately 2 W power dissipation in an atmosphere. This energy must be dissipated. If this can be achieved needs to be tested in a vacuum chamber.

Also, the standard installed electrical components are not radiation hardened for the use in space. Optotune offers the possibility to exchange some parts, but this does not lead to a system robustness to radiation. Either some components have to be exchanged or a form of shielding needs to be incorporated to protect the electronics.

The MR-15-30 is not space certified. While it can withstand temperature swings from -20℃ to 90℃, shocks of 105g, and vibrations of 2g with a resonance of 10-150 Hz, it is not designed for use in a vacuum. The joints use grease, which is not vacuum compatible. It would lead to outgassing, controllability issues, and eventually to parts failure. A change of the lubricant will not be possible without significant development and testing by the manufacturer.

Another aspect of concern is the system's thermal envelope. it has not been tested to dissipate the power loss purely through radiation. As the mirror withstands approximately 2 W power dissipation in atmospheric conditions same must be tested successfully under vacuum.

Furthermore, the standard installed electrical components are not radiation hardened for the use in space. Optotune offers the possibility to exchange some parts, but they are not proven to lead to a satisfactory robustness to radiation. Either some components have to be exchanged or a form of shielding needs to be incorporated to protect the electronics.

3 Test Build

Due to the fact that Newson or Optotune do not provide complete documentation regarding the behavior and performance of their mirror systems, a test track needed to be set up. A test track was therefore designed to thoroughly characterize the mirror systems. It consisted of THORLABS equipment, which is further described in 3.1.

The following four underlying questions need to be studied with this setup:

1. What is the step and frequency response of the actuators?
2. Is the actuator response linear?
3. Is the response linear throughout the entire movement range?
4. Is the mirror system space compatible?

The compact setup of the test track allowed the optical elements to be tested in space-like environments. It can be placed into a vacuum and radiation chamber and onto a vibration table. This was crucial since Newson and Optotune has not performed these tests in accordance to the DLR requirements. Through these tests it is also possible to determine the performance of the internal feedback control loop for external disturbances.

Another side benefit of this setup is its modularity. The Newson system can easily be exchanged for a different mirror system and therefore provide a stable and fast platform to test and integrate other mirror systems, making it available for future projects at the DLR.

3.1 Setup

The entire setup is built on top of a ”breadboard” system from THORLABS. This is a standardized and modular system, which provides simple assembly and great flexibility through a big number of available parts. The DLR has been using this system for numerous applications and the knowledge and experience amassed herewith, as well as the readily available parts were a welcome support. The final parts Bill of Materials for the test rack can be found in Appendix B and Figure 3.14 shows the final assembled test track.

The test track is connected to three elements, as shown in Figure 3.1. The Speedgoat is a real-time target computer designed to work together with MathWorks Simulink. Together, they form a complete environment for rapid control, hardware-in-the-loop simulation. It controls the DEMCON mirror, used in the verification process described in 3.5, and logs data from the mirror and the laser beam sensor described in 3.1.3. The power supply modules provide power to the laser beam sensor and the mirror. The external laser source, described in 3.1.1, generates the laser for this experiment.

The developed test track is broken down into four main parts: a laser collimator, the Newson Mirror system, a sensor which measures the laser beam deviation, and a $4f$-Relay. Each of these components are described in the following sections. These were designed separately and then assembled together as shown in Figure 3.2.

3.1.1 Laser Collimator

The laser beam is generated through a fiber-coupled laser source which is then focused on infinity with a collimator. This generates nearly parallel light rays which are ideal for optical tests. They also mimic the laser rays of the ISL terminal in space.

Figure 3.1 Schematic view of the test track set up

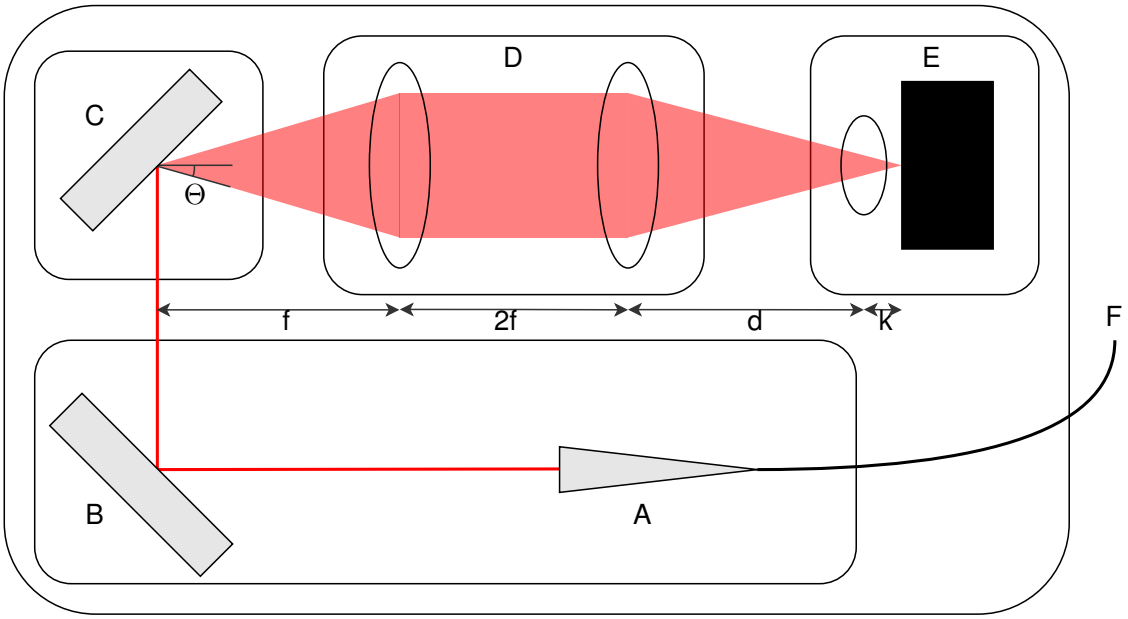

Figure 3.2 Schematic view of the test track consisting of A: collimator, B: stable mirror, C: testing mirror, D: 4f-Relay, E: focus lense and laser beam sensor and F: laser fiber

The THORLABS *S3FC1550* laser was used in this setup. It generates a laser beam with a wavelength of $1540nm$ which travels through an FC/PC-terminated fiber and is power adjustable. $1540nm$ is the mean wavelength used in the ISL Terminal and is therefore the right source to represent real use cases.

The chosen collimator is the *F260FC-1550* from THORLABS. This fiber collimation package is pre-aligned to collimate light from an FC/PC-terminated fiber with diffraction-limited performance. Because these fiber collimators have no movable parts, they are compact and easy to integrate into an existing setup. Due to chromatic aberration, the effective focal length of the aspheric lens is wavelength dependent. Therefore, a collimator optimized for $1540nm$ was chosen. In addition, the aspheric lens has an antireflective (AR) coating on both sides that minimizes surface reflections, which is made from hard refractory-oxide. Another selection criteria was the generated collimated beam diameter. The *F260FC-1550* has a beam diameter of $3.0mm$. This simulates the laser of the ISL Terminal and is therefore as close to reality as possible.

The implementation of the collimator into the THORLABS test track is is relatively straightforward. An adapter accepts the collimator and is then placed into a kinematic mount. It enables precise angular alignment of the beam along the axis of the light. This mount is then connected to a height-adjustable stand. Through the use of an adapter, the collimator can easily be replaced for different laser wavelength tests without the need to exchange the entire kinematic mount and need to repeat the alignment process.

A $45°$ mirror (B in Figure 3.2) was added to the collimator setup. This mirror deflects the laser by $90°$, before it hits the Newson Mirror System. While this deflection is not needed, it adds the possibility to replace the mirror with an FSM. The FSM can then be used to introduce disturbances, such as random small movements resembling vibrations, to the system and test whether and how the to-be-tested mirror

responds to such conditions. The mirror chosen is a 2 inch silver coated mirror that was available at the institute. The silver coating has been testes to perform well enough in the infrared spectrum of 1050-1700 nm for these tests.

3.1.2 Mirror Holder

Due to the Newson mirror system's big diameter of 60 mm, it was not possible to mount it within THORLABS parts. Therefore, a separate housing solution was designed. On the outside of the mirror, a rim extends 2mm, as seen in Appendix A.1. This is used to keep the mirror from sliding out of its circular housing. Furthermore, there is an alignment notch at the crest of the rim. It prevents the mirror from turning around its own axis. The top mirror holder has an inversion of the notch, which holds it in place. Both halves are being held together by an M3 screw and M3 nut. The nut is being held in place by the bottom holder, while the screw tightens from the top. This approach simplifies the handling of the mirror and is structurally stronger and more secure than using screws that drive into 3D printed parts, as plastic can degrade with multiple screw-ins.

The first iteration of the mirror holders can be seen in Figure 3.3. The parts were printed on a Formlabs Form2 SLA printer at the institute. The final design is discussed in Section 3.3. The changes in design from Figure 3.3 to Figure 3.12 have to due with space limitations and minimizing uncertainties in the test track. They will be described in more detail in Section 3.2 and 3.3.

The Optotune mirror has an M3 screw thread incorporated into its housing. This simplifies the integration of the mirror into the test track greatly. Yet, the Optotune mirror has to be connected to the test track. For this purpose, a mirror holder for the Optotune mirror was also designed. By the time this mirror holder was designed, the final iterations of the Newson mirror holders were already produced. Therefore, the first design of the Optotune mirror holder took the adjustments from Section 3.2 and 3.3 into account. The only and final Optotune mirror holder is pictured in Figure 3.12

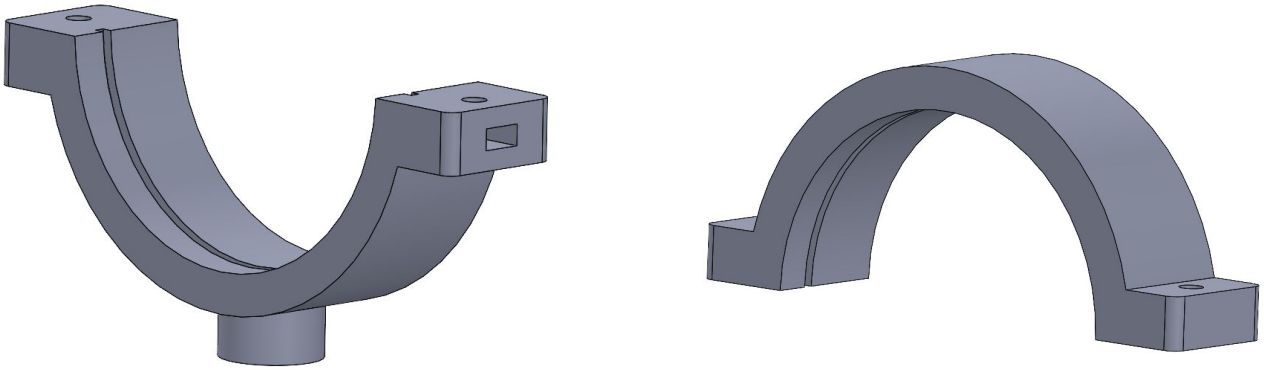

(a) Bottom Mirror Holder **(b)** Top Mirror Holder

Figure 3.3 First iteration of Newson Mirror Holders

3.1.3 Laser Beam Sensor

The movement of the laser is being detected with a position sensitive detector (PSD) . PSDs are opto-electronic position sensors that utilize photodiode surface resistance. They provide continuous position data, high position resolution, and a high-speed response. The specific PSD used in this experiment is the *IGA-050-PSD-E4* tetra lateral photodiode from Electro-Optical Systems.

Lateral effect PSDs use a continuous single element, planar diffused photodiode with no gaps or dead areas. Therefore, they can provide a direct readout of a light spot across their entire active area. This is achieved by providing an analog output directly proportional to both the position and intensity of a light spot. A light spot on the active area generates a photocurrent, which flows through the resistive

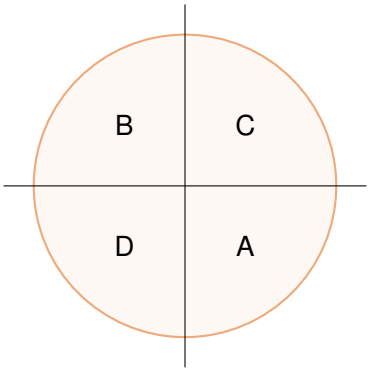

Figure 3.4 Alignment of the quadrants of the PSD

layer to the four contacts. There are four contacts attached to the active area, which divide the active area into four imaginary quadrants, as shown in Figure 3.4. The generated photocurrent is inversely proportional to the resistance between the incident light spot and the contact. A light spot at the center of the photodiode generates equal currents in all contacts. By moving the spot, the change in current can be used to determine the exact light spot position at each instant of time. These electrical signals are proportionately related to the light spot position from the center [29].

An advantage of the lateral effect PSDs is that they are not limited on the input light beam's shape and size since the electrical output signals are proportional to the displacement from the center. As a result, these devices can resolve positions with an accuracy of less than $0.5\mu m$ [29].

The PSD used in this setup has an active diameter of 5mm and an accuracy of less than 1 µm by $0.1mW$ incident power. While the active area is one piece, the PSD generates one photocurrent for each quadrants of the active area. The photodiode is attached to a PCB which generates usable signals out of the photocurrents and provides the PSD with power. This PCB was already available at the institute and not designed for the scope of this thesis. The combined PSD and PCB assembly was mounted into a THORLABS translating mount, which allows 2 axis adjustment for accurate implementation into the test track.

In order to get a light spot to hit the PSD, the laser needs to be focused with a lens. Since the angular field of view (AFOV) and the sensor size H is known, the ideal focal length f_{ideal} for the lens can be calculated by using

$$f_{ideal} = \frac{H_{1/2}}{\tan(AFOV)} \tag{3.1}$$

[15]. With an AFOV of $40°$ optical and half a sensor size of $H_{1/2} = 2.5mm$, f_{ideal} becomes $2.98mm$. Lenses with such a sort focal length have a very small diameter. THORLABS does not offer a suitable lens for this application. This was one of the reasons along with others discussed in more detail in 3.2, why it was decided not to test the entire mirror's AFOV at once, but rather spilt it in $+10°$ and $-10°$ AFOV. With the new AFOV being $20°$, f_{ideal} now becomes $6.87mm$. For this focal length, focus lenses with an adequate diameter were available. It was then mounted onto a THORLABS lens holder and mounted coaxial to the PSD.

3.1.4 4f-Relay

Due to the small active diameter of the PSD, the small diameter of the focus lens, and the big angular movement of the mirror system, it became apparent that it will be extremely difficult to reliably hit the focus lens with the moving laser. The large PSD mount, in combination with the large diameter of the Newson mirror and its holder, made it impossible to move the sensor close enough to the mirror to hit the PSD through the entire movement range of the mirror. As a result, a new approach had to be used.

An optical relay system can be used as a suitable means to move the PSD further away from the mirror. This consists of a pair of fixed, coaxial mounted lenses. The lenses are thin and convex with focal lengths

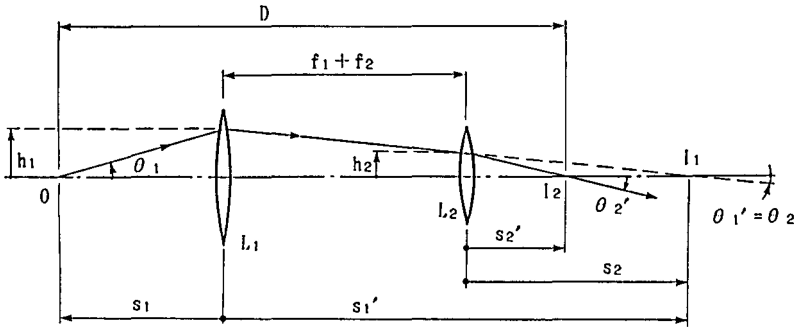

Figure 3.5 $4f$-Relay with two different focal lengths [11]

f_1 and f_2 and are separated by the sum of their focal lengths. The lateral, axial, and angular magnifications of this system, denoted as M_{lat}, M_{ax}, and M_{ang}, respectively, are represented as follows:

$$M_{lat} = -f_2/f_1 \tag{3.2}$$

$$M_{ax} = (f_2/f_1)^2 \tag{3.3}$$

$$M_{ang} = -f_1/f_2 \tag{3.4}$$

The total distance D from the object to the final image is given by:

$$D = (f_1 + f_2)^2/f_1 + [(f_1/f_2)^2 - 1]s_1, \tag{3.5}$$

where s_1 is the distance from the first lens in the system to the object. s_1 is negative, since the positive direction is defined as the direction light waves travel through the system [11]. Figure 3.5 shows an optical relay system with two lenses with different focal lengths.

If the focal lengths of the two lenses are the same, $f = f_1 = f_2$, then (3.5) becomes independent from s_1 and D equals $4f$. As a result, the object is being relayed at the $4f$ distance along the axis from the original place, regardless of the object's distance to the first lens. The name "$4f$-Relay" comes from this property.

The magnifications are also independent from s_1. Therefore, their values become

$$M_{lat} = -1 \tag{3.6}$$

$$M_{ax} = 1 \tag{3.7}$$

$$M_{ang} = -1. \tag{3.8}$$

The relay does not distort the image but only mirrors it. As a result, the $4f$-Repay can theoretically be used to extend the working distance in the test track without changing the angles of light. It is placed between the mirror and the PSD, as shown in block D of Figure 3.2.

Lens Selection

The lens selection plays an important role in the performance of the $4f$-Relay. Optical instruments can ideally give stigmatic images of points on a single surface. In reality, however, inaccuracy in the lens shape and its material characteristics may cause a quality degradation in the image. This departure from the ideal image is known as *aberration*. Aberration can be tolerated to an extent, but should be suppressed below a tolerable level [13].

There are two main types of aberration: chromatic and monochromatic. Due to the use of a single wavelength laser, only monochromatic aberration is of interest; monochromatic aberrationcan be further divided into aberration that deteriorates the image quality — spherical aberration, coma, and astigmatism — or aberration that deforms the image — Petzval's image field curvature and distortion [14]. In this

experiment, only spherical aberration will be considered, since it is the only aspect, that can be controlled the best.

Spherical aberration defines the magnitude light rays are bent beyond the focal point of a lens. The further away a ray of light hits the area of a lens away from its center axis h, the more it will be bent towards its focal point. This is shown in Figure 3.6. As h increases, the refraction of the light rays increases. As a result, the light is not focused on one single point anymore and its energy density decreases. This augments the spot size and can cause inaccurate PSD readings, since a bigger spot might not completely hit the active area.

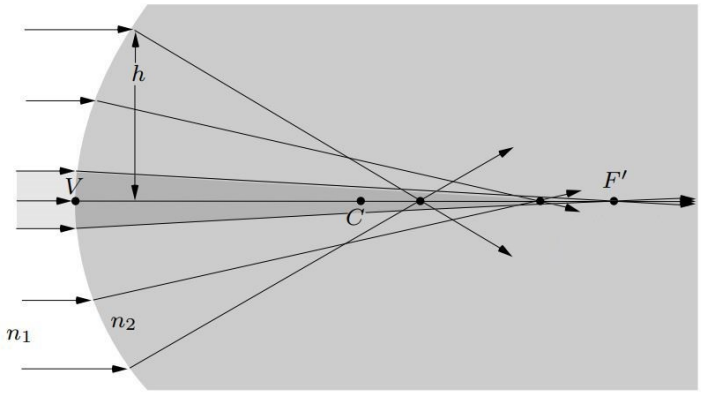

Figure 3.6 Spherical aberration at the surface of a lens [14]

This behavior can be counteracted by choosing the right lens type. If the lens is generally seen as a combination of two prisms whose surface areas are connected, the incident ray is minimally deflected if its angle is approximately the same as that of the outgoing ray. If the incoming light is parallel, a simple diverging or converging lens with an almost flat back exhibits minimal aberration. A combination of a converging and a diverging lens (an achromatic doublet) can also be used [14].

According to [4], the reciprocal of the focal length of a combination of two thin lenses separated by a distance l is given by

$$\frac{1}{f} = \frac{1}{f_1} + \frac{1}{f_2} - \frac{1}{f_1 f_2}. \tag{3.9}$$

Aberration can be reduced if these two lenses are put in contact, creating an achromatic doublet. Then, $l = 0$ and using 3.9 one gets

$$\frac{1}{f_1} = \frac{1}{f}\frac{\Delta_2}{\Delta_2 - \Delta_1}, \quad \frac{1}{f_2} = -\frac{1}{f}\frac{\Delta_1}{\Delta_2 - \Delta_1}, \tag{3.10}$$

where Δ_1 and Δ_2 is the dispersive powers of the two lenses. For a given glass and a fixed value for the focal length f, f_1 and f_2 are specified uniquely by 3.10. Since f_1 and f_2 depend on three radii of curvature, one can be chosen arbitrarily. This degree of freedom makes it possible to minimize spherical aberrations as much as possible.

Therefore, the two lenses in the $4f$-Relay were chosen to be achromatic doublets from THORLABS. They have an AR coating that is designed for use in the infrared spectral region of 1050-1700 nm. The achromatic doublet lenses from THORLABS have a 7-fold reduced sensitivity to centration on the beam axis when compared to spherical singlets and aspheric lenses, as can be seen in Figure 3.7. A focal length of $f = 35mm$ was chosen due to size constrains of the THORLABS breadboard, on which the system is built, and since it was the minimal distance the lens could be away from the Newson mirror system.

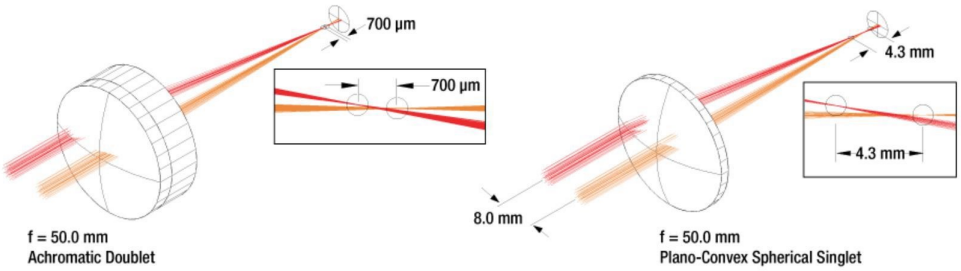

Figure 3.7 THORLABS achromatic doublet lenses great off axis performance [28]

3.2 Optical Simulations

Before ordering the parts and building the test track, the design had to be validated. The optical software *OpticStudio* by Zemax was used to create a simulation environment of the designed test track. For the lenses and collimator, supplied by THORLABS, the Zemax files in *.zar* format are available on the supplier's website and could be directly integrated into the simulation. The $45°$ mirror from 3.1.1, the PSD active area, and the NMS were modeled separately. The size of the collimated laser needed to be calculated separately as well. This can be done with

$$d_{collimator} = f * \theta_{fiber} \approx f * \frac{\lambda}{\pi d_{fiber}}, \tag{3.11}$$

with θ_{fiber} being the beam divergence half-angle and d_{fiber} the diameter of the fiber from the laser source [22].

OpticStudio has the ability to add mirrors into a simulation. The $45°$ mirror was so added with its diameter of 2 inches. The NMS had to be modeled with its range of motion. First, the entire AFOV of $\pm 13.5°$ was tested with the chosen lenses for the $4f$-Relay, from 3.1.4, with a diameter of 1 inch. The simulation showed that the large angular movement hindered the laser from hitting the second lens of the $4f$-Relay, as seen in Figure 3.8. The three strands simulate the laser without any deflection (middle) and with the maximal deflection of $\pm 13.5°$ (top and bottom).

To overcome this issue, the 1 inch lenses were switched out with 2 inch lenses. Their focal length is 75 mm, which is the shortest focal length available. However, due to this now longer length, the possible advantage of the 2 inch diameter is lost. The laser rays do not pass through the clear aperture (CA) of the lens, which is 90 % of the diameter, so 45.72 mm, as shown in Figure 3.9. This leads to an increase in spherical aberrations, which would degrade the beam quality. The extreme deflection cases also do not hit the active area of the PSD, making the 2 inch lenses not a viable option for the $4f$-Relay.

As a result of these simulations and the focal length problems in 3.1.3, it became apparent that the entire range of motion of the NSM could not be tested in one setup. Therefore, these tests were split into two AFOV sections: $-13.5° \leftrightarrow 0°$ and $0° \leftrightarrow +13.5°$. During each test, the NMS now has a range of motion of only $\pm 6.75°$. Instead of positioning the NMS at an angle of $45°$ to the laser, it is now positioned at an $38.25°$ and $51.75°$ angle for the $-13.5° \leftrightarrow 0°$ and $0° \leftrightarrow +13.5°$ ranges, respectively.

Figure 3.10 shows the simulation for the $-13.5° \leftrightarrow 0°$ scenario. The $0° \leftrightarrow +13.5°$ scenario is identical to Figure 3.10. It is clear, that the laser goes through the CA of the lens, minimizing spherical aberrations. All beams hit the focus lens through its CA, and the focused spot hits the active area of the PSD.

The simulation was run with two different focus lenses; one with a diameter of $d = 5mm$ and a focal length of $f = 7.5mm$ and one with a diameter of $d = 8mm$ and a focal length of $f = 10mm$. The idea being, that it will provide more flexibility during testing, in case unforeseen disturbances emerge in the setup. While both focal lengths focus the spot onto the PSD, the longer focal length uses the entire diameter, as seen in Figure 3.11. Therefore, the $d = 8mm$, $f = 10mm$ lens can provide more accurate resolution of the NMS movement, but might not work at the extreme angular deflection cases, if it is not possible to focus the spot perfectly. Both the focal lengths are not the ideal focal length of $f_{ideal} = 6.87mm$ calculated in 3.1.3, but the only available lenses with a similar focal length.

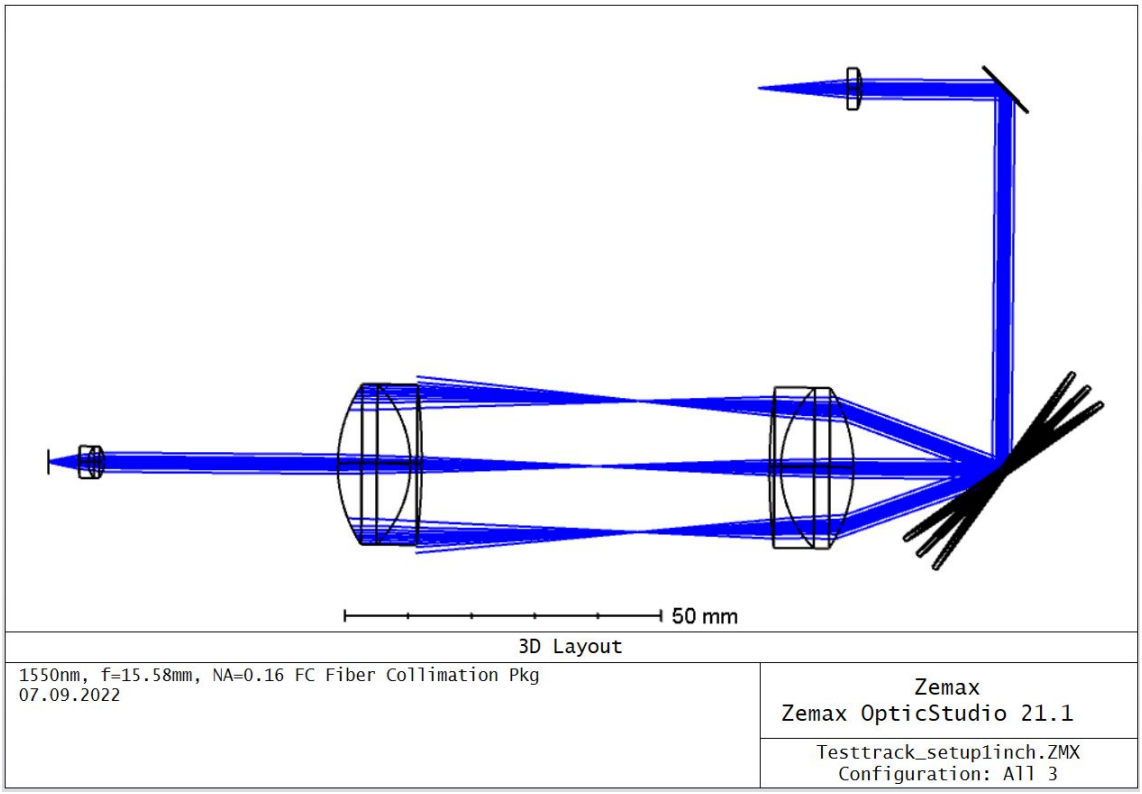

Figure 3.8 Failed simulation of full AFOV with 1 inch, $f = 35mm$ lenses

The simulations calculated the optimal distance d and k from Figure 3.2 in order to generate a focused spot on the PSD. These measurements were used to set up the track correctly and simplify the alignment process. Finally, these simulations prove that the $4f$-Relay can be used to increase the distance between the NMS and the PSD, while maintaining the angular offsets the mirror creates.

3.3 Uncertainty Analysis

In this section, potential error sources and their uncertainties are analyzed for the evaluation of the final measurement. There are two dominant error sources in the test track: the PSD measurement and misalignment of the optical system. Under the assumption that all error sources are independent, the standard deviation of the beam displacement error can be written as

$$\sigma_{p_\theta}^2 = \sigma_{PSD}^2 + \sigma_{opt}^2, \tag{3.12}$$

where σ_{PSD} and σ_{opt} denote the standard deviation caused by PSD and optical alignment, respectively [31]. Both error sources will be discussed in the following sections.

3.3.1 Uncertainty in PSD Measurements

The PSD is the main sensor of this setup and therefore errors in PSD measurements need to be analyzed. These can be broken down into three error sources, which are a scale error, a precision error, and an accuracy error. First, the scale error of the PSD is the error in scaling of the PSD position calculation. This error can be caused by the inaccurate calibration of the PSD, gain mismatch in analog units, and temperature variation. Secondly, the precision error is an uncertainty of the PSD measurement by the noise of the signal, which changes with the bandwidth. Last, the accuracy error is the error due to the distortion of the PSD measurements. It can be defined as a residual position error or nonlinear distortion after the correction of the scaling error.

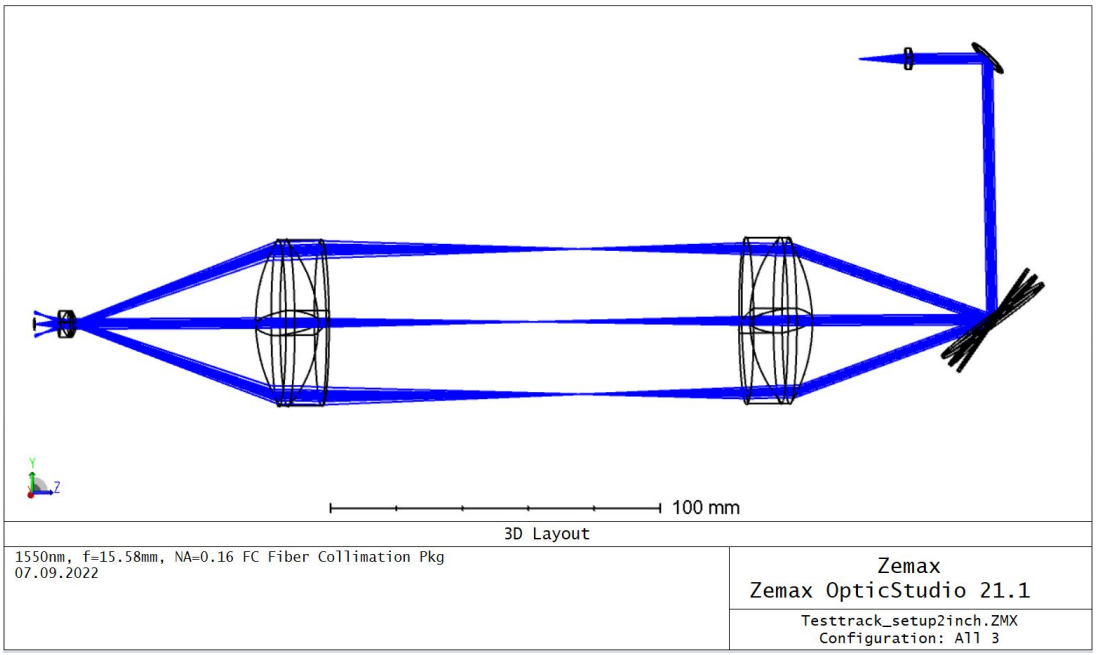

Figure 3.9 Failed simulation of full AFOV with 2 inch, $f = 75mm$ lenses

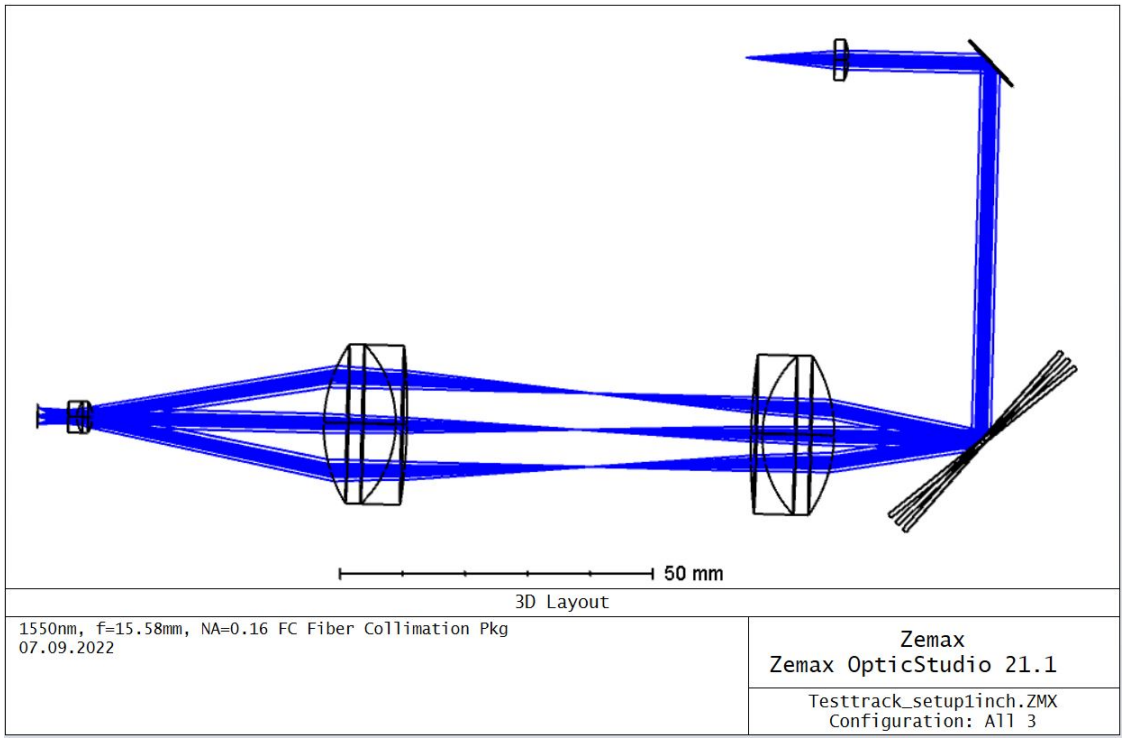

Figure 3.10 Simulation with $\pm 6.75°$ range of motion with 1 inch, $f = 35mm$ lenses

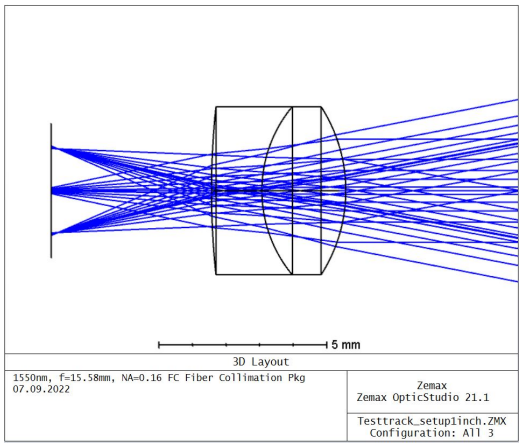

(a) $d = 5mm$ and $f = 7.5mm$ with not optimal active PSD area utilization

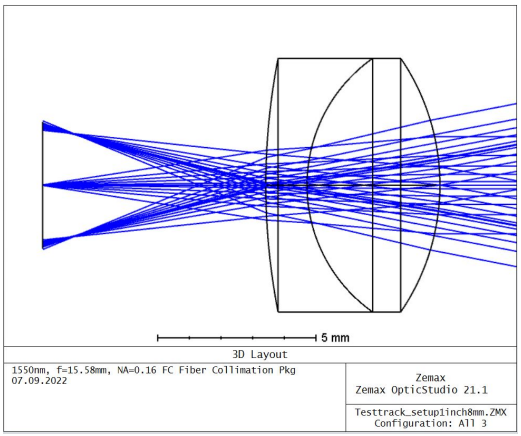

(b) $d = 8mm$ and $f = 10mm$ with maximal active PSD area utilization

Figure 3.11 Comparison of active PSD area utilization

3.3.2 Uncertainty in Optical Alignment

To understand the alignment of the optical components, it can be best described in a local coordinate system. Every part has three coordinates and a rotational component. For example, at the laser collimator, x_l is aligned with the beam direction, z_l is orthogonal to the breadboard, and y_l is orthogonal to x_l and z_l, which is parallel to the breadboard surface. For the mirrors, the PSD, the $4f$-Relay and focus lenses the normal vector of the surface plane is aligned with x_m, x_{NMS}, x_{PSD}, x_{4f1}, x_{4f2}, and x_f axis, respectively. The axes for other components are defined in the same manner. For all defined axis, for example x_l, the translation positions errors and the rotational errors are defined as d_{x_l} and δ_{x_l}, respectively [31].

Through these coordinates, the ideal alignment can be defined in four conditions:

1. The height of the laser, the mirrors, lenses, and PSD are at the same height and the beam stays parallel to the breadboard. This leads to

$$d_{z_l} = d_{z_m} = d_{z_{NMS}} = d_{z_{PSD}} = d_{z_{4f1}} = d_{z_{4f2}} = d_{z_f} \text{ and } \delta_{y_l} = \delta_{y_m} = \delta_{y_{NMS}} = 0. \tag{3.13}$$

2. The laser hits the center of the NMS where the rotational axis is located, i.e. $d_{y_l} = d_{y_m} = 0$.

3. The laser from the NMS is perpendicular to the y axis of the PSD, meaning $\delta_{z_{PSD}} = \delta_{z_{NMS}} = 0$ and is parallel to the axis of the $4f$-Relay and focus lens.

4. Lastly, the distances between the $4f$-Relay lenses and their objects is equal to their focal length.

To minimize each of these three error sources, multiple solutions were considered. The height problem was solved by using THORLABS' optomechanical cage system. This makes it possible to mount components onto a rail system, that holds everything aligned. As described in Section 3.1, the test track consists out of four separate parts. Therefore, multiple cage system had to be designed. The first cage consisted of the collimator and the $45°$ mirror, making $d_{z_l} = d_{z_m}$ as well as $d_{y_l} = d_{y_m} = 0$. The second cage helped align the PSD with its focus lens and the two $4f$-Relay lenses, i.e. $d_{z_{PSD}} = d_{z_f} = d_{z_{4f1}} = d_{z_{4f2}}$ and $d_{y_{PSD}} = d_{y_f} = d_{y_{4f1}} = d_{y_{4f2}} = 0$. The NMS´s diameter of 60 mm was too large to fit into the 60 mm cage system. A separate solution was designed, described in the next paragraph. The two cage systems could still be at different heights and angles to each other. To minimize errors between the cages, an interconnection was added. It used right-angle kinematic mounts and rods to connect the two cages. This led to $d_{z_{CAGE1}} = d_{z_{cage2}}$ and $\delta_{z_{CAGE1}} = \delta_{z_{cage2}} = 0$. To satisfy the horizontal beam requirement, each cage was connected to the breadboard by two pillars each. This minimized their rotation around the y axis.

The NMS cannot use THORLABS parts to be integrated into the system. As a result a custom solution was designed, as was described in 3.1.2. These parts were redesigned to make it possible to integrate

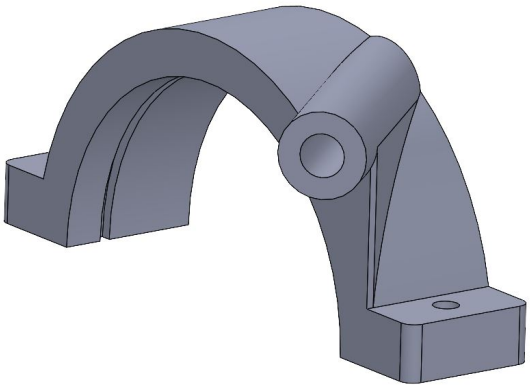

(a) Top mirror holder with $38.25°$ offset

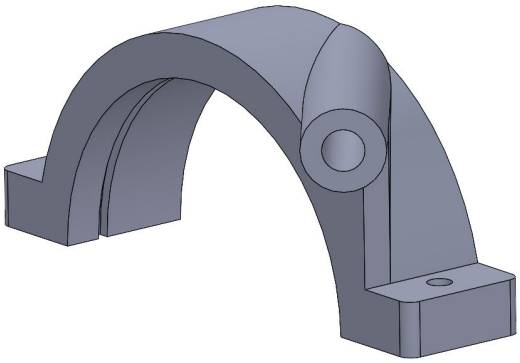

(b) Top mirror holder with $51.75°$ offset

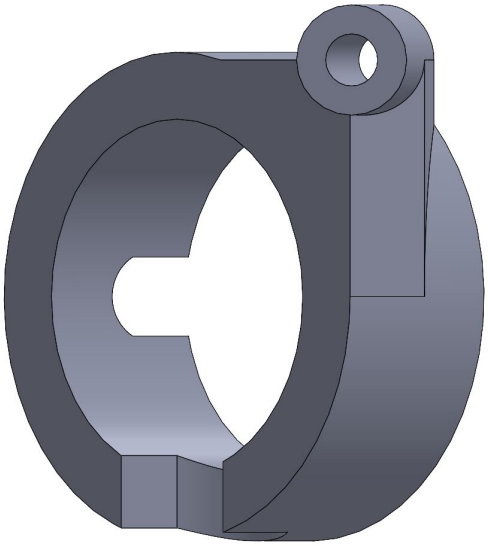

(c) Optotune mirror holder with $38.25°$ offset

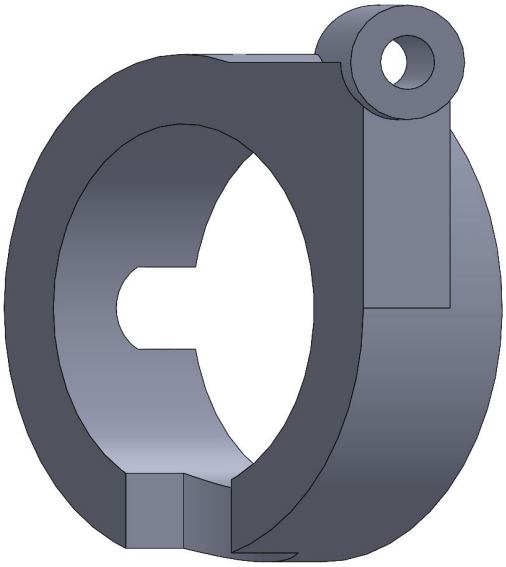

(d) Optotune mirror holder with $51.75°$ offset

Figure 3.12 Final iteration of the top Newson mirror holder and the Optotune mirror holder

the NMS into the cage system. One of the cage system rods is extended toward the NMS and threaded into a mount. Therefore bringing everything onto the same height level, i.e. $d_{z_{cage1}} = d_{z_{cage2}} = d_{z_{NMS}}$. The rod also limits the rotation of the NMS around the z axis. It also provides the opportunity to control the angular offset of the NMS to the laser. The two angular scenarios described in Section 3.2 could be implemented while minimizing the rotational errors. The top mirror holder was redesigned in such a way, to create a $38.25°$ and $51.75°$ offset to the laser. As a result, for each scenario a separate mirror holder is being used. The two new holders are shown in Figure 3.12. The bottom mirror holder stayed identical to Figure 3.3a.

The Optotune mirror used the same concept to integrate into the test track and limit its uncertainties. Here as well, two holders are designed to create a $38.25°$ and $51.75°$ offset to the laser. The holders are shown in Figure 3.12.

The last condition, optimal lens distances, for an ideal alignment can be achieved by using a THORLABS rod with distance scaling engraved. With it, the $4f$-Relay lenses could be moved to the right position within the cage system and actually create an optical relay with a relay-distance of $4f$, or 140 mm.

3.4 Electronics

To make the test track fully operational, the mounted electronics had to be controlled. The PSD needs to be powered and its position values communicated to the lab equipment. The NMS also needs power and its communication hardware.

As described in 2.3.3, the NMS needs external electronics to modulate the communication data onto the power supply. The connection between the NMS and the PCB is made via SubMiniature version A (SMA) connectors. These were also used to connect the RX and TX signals to the lab equipment. SMA connectors were chosen since they are the common and most versatile connector in conjunction with the lab equipment. The board uses 12 V directly from the ISL Terminal to supply the mirror and 5 V to modulate the signals onto the power supply. Since the ISL Terminal supply voltage is 12 V, it could be used directly. An unregulated, isolated DC/DC converter converts the supply voltage to the needed 5 V. The soldered PCB was tested using a frequency generator to confirm its basic functionality and to test the components. The final NMS PCB is shown in Figure 3.13a.

A small PCB was designed for the PSD to have three functions. First, it accepts the Molex-Connector from the PSD board in the cage system and makes it possible to transfer information and provide power. Second, the PSD readings are transferred from the Molex connector to four SMA connectors. This enables connectivity to the lab equipment for accurate data logging. The SMA cables were connected to the Speedgoat computer of Figure 3.2 and the outputs were sampled at 10 Hz. Third, the PSD requires stable $\pm$ 5 V. The 12 V used on the NMS board is used with the PSD PCB. This reduces the need for multiple voltage sources, which is desired to minimize the hardware usage during testing. The 12 V is reduced to 5 V using a Low Dropout Voltage Regulator. These 5 V are then fed into a fixed negative 5 V output inverting DC/DC converter, which is integrated into a supplier provided circuit. The extra circuit maximizes noise immunity and protects the converter. At the end, the $\pm$ 5 V is routed through an analog supply filter to further minimize disturbances. The final PCB is shown in Figure 3.13b.

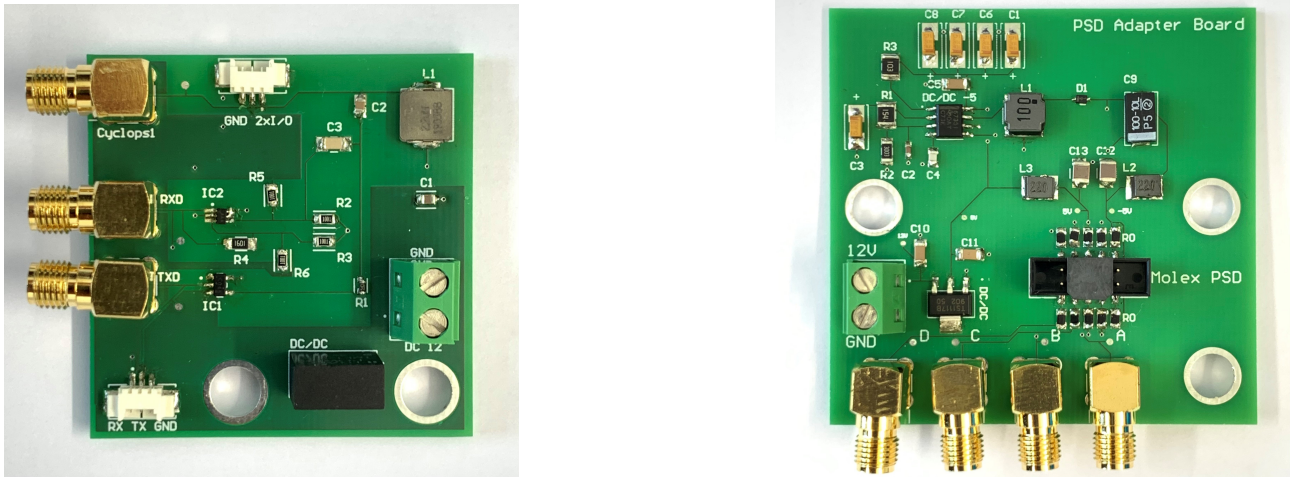

(a) NMS electronics control board

(b) PSD control board

Figure 3.13 PCBs used to control the electronics on the test track

3.5 Verification

Before the Optotune mirror can be tested, the PSD and the design of the $4f$-Relay need to be verified. First, the PSD was evaluated to understand its behavior and then the laser movement through the test track could be checked. There are three variables within the test track that can affect the outcome of the verification process: the Optotune mirror, the $4f$-Relay, and the PSD. Each component needs to be tested separately, to be able to analyze its behavior without being influenced by the others.

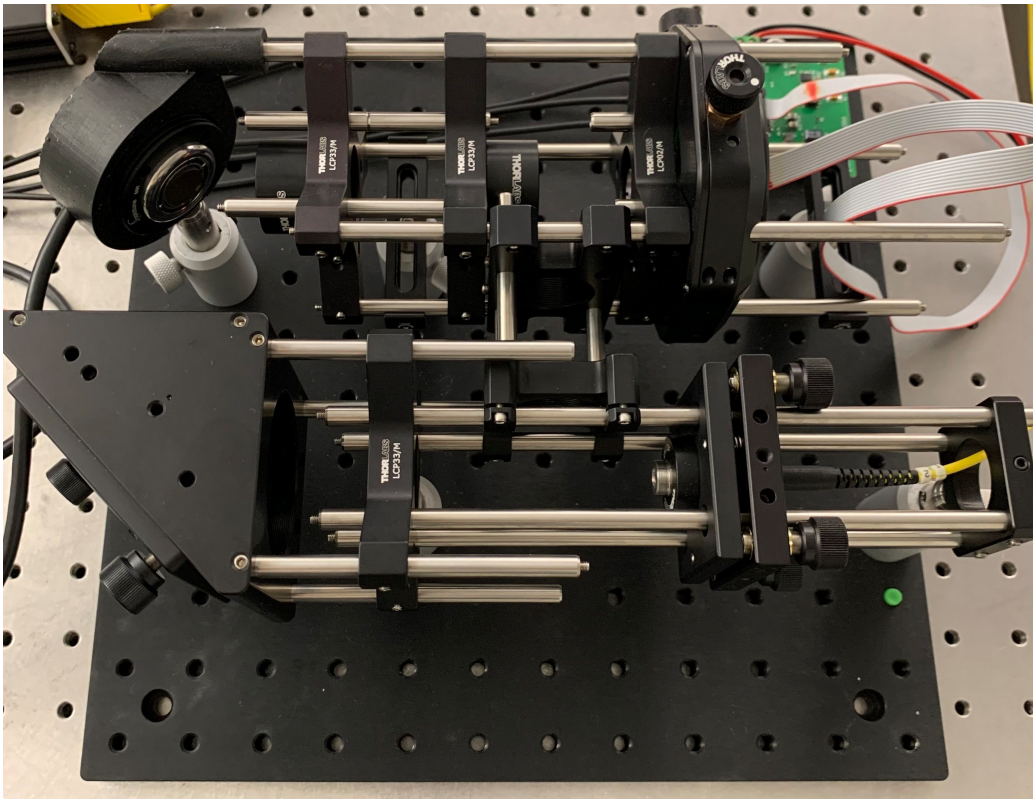

Figure 3.14 Fully assembled test track with the Optotune mirror in its mirror holder

In the first step, the FSM from the company DEMCON replaced the Optotune mirror. The DEMCON's movement range is $\pm 1°$, yet only $\pm 0.6°$ were used, since the developed feedback control works best within this range. In relation to the other systems, this is a very small angular movement, but sufficient to test the PSD and the $4f$-Relay. Since the DEMCON FSM has been successfully tested in past projects and can be controlled with high precision, it was used to analyze the outputs of the PSD through its movement range. The DEMCON FSM is controlled through the attached Speedgoat computer. The angular mirror movements are input there, as well as, the internal control loop samples and adjusts the actual mirror position to the applied values at a rate of 20 kHz. Although the control feedback loop works very fast, the mirror input values are not adjusted at 20 kHz. This is because of the maximum controllable adjustment speed of the FSM is $0.1°/s$. Due to the orientation of the DEMCON FSM in the test track, its x axis and y axis are orientated differently. From now on, the coordinate system in Figure 3.15 will be used as standard.

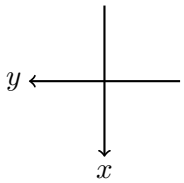

Figure 3.15 Orientation of DEMCON FSM axes

Since the $4f$- Relay cannot be tested without the PSD, the PSD was verified first. Therefore, the $4f$-Relay was removed temporarily from the setup and the laser went directly to the PSD from the DEMCON FSM. Just a focus lens was used to focus the incoming beam in the active area.

3.5.1 PSD

There were two main problems with the PSD. First, due to its mounting in an adjustable holder in the test track, the active surface is not aligned with the optical axis of the laser. Second, no documentation exists about its specific behavior and therefore some phenomena, which occurred during the first tests, could not be explained through simple inspection.

Basic Alignment

Since the photocurrent of each sector of the active area is proportional to its incoming light, one can assume that once all photocurrents are equal, the focused laser hits the PSD in its center. For this to be true, however, the photocurrents cannot have an offset to each other. While not shining a laser on the active area of the PSD, each sector produced an anomalous photocurrent. This is shown in Figure 3.16, where the voltage outputs of the amplifiers are measured.

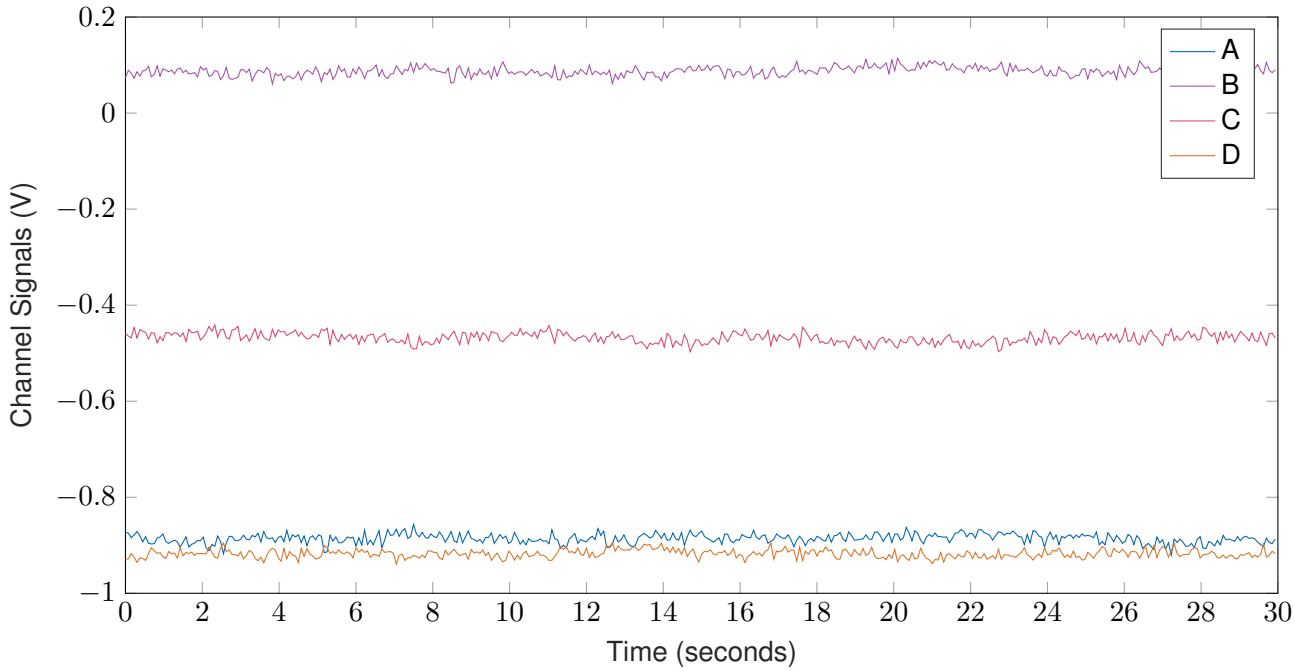

Figure 3.16 Voltages of the amplified photocurrents of all PSD quadrants without an active laser

It is clearly visible, that each channel contains large deviations from one another. This behavior did not change once the entire test track was covered, so that outside light pollution could not interfere with PSD measurements. Therefore, these currents must be produced within the PSD or its amplifiers and is considered noise.

At first, it was not clear, if these voltage deviations had an effect on the PSD once a laser is shined onto it. Therefore, a laser was calibrated through the center of the test track and the DEMCON FSM was regulated to have $0°$ angular offset. The PSD was then adjusted in the vertical and horizontal axes until all voltage readings were identical. Visual inspections showed that the PSD was not centered around the optical axes of the test track. As a result, the need for a more detailed evaluation of the PSD became apparent.

Further Evaluation

In order to gain a better understanding of the behavior of the PSD, the entire active area had to be evaluated. A common procedure to characterize PSDs is to scan the active area with a grid pattern. For this approach, the $\pm 0.6°$ movement of the DEMCON mirror needs to be enough to cover the entire active area

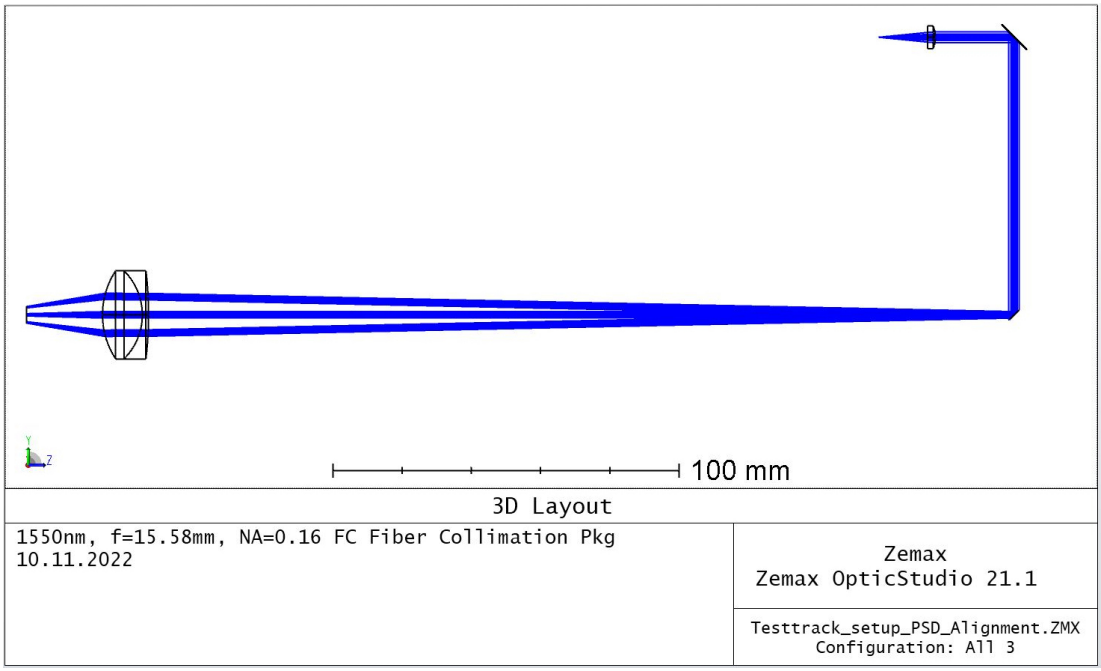

Figure 3.17 Simulation with $\pm 0.6°$ range of motion with 1 inch, $f = 35mm$ lens for PSD characterization

of the PSD. A large distance between the mirror and the PSD is needed to produce this range of motion. A new simulation, as shown in Figure 3.17, was undertaken to find the distance, where the entire active area of the PSD is covered by the mirror's movements of $\pm 0.6°$. The focus lens was moved 310 mm away from the DEMCON FSM. The focus lens, on of the $4f$-Relay lenses, is 31 mm away from the PSD, so that a focused spot hits the PSD.

A complete pass of the active area produced the voltage distribution shown in Figure 3.18. The circular active area of the PSD is clearly visible, yet, it also shows that some disturbances occur in the bottom corners. These can be caused by either light refraction at the focus lens or at the cover glass of the PSD or through malfunctioning components. The light refraction at the focus lens is very unlikely, since the THORLABS lens has a special AR coating to reduce aberrations and retractions and is optimized for the IR spectrum. It is also unlikely that the cover glass of the PSD causes this issue, since this would be counterproductive from a design perspective. Due to the large distance between the focus lens and the DEMCON FSM, the PSD and the focus lens were not over the THORLABS breadboard of the test track. While still mounted in the cage, they were suspended at a significant distance from the last mounting point. This approach was necessary to achieve the specified distance of 310 mm, while still benefiting from the alignment the cage provides. As a result, the PSD and focus lens could be sagging and causing the light to hit the lens at non desired angles of incidence. Disturbances could be caused through this. To check whether the PSD is faulty, a different approach was chosen.

The focus lens and the PSD were moved closer to the DEMCON mirror and the distance between the PSD and the focus lens was also reduced. As a result, the laser did not hit the PSD as a collected small spot, but rather as a larger diffused circle. Yet, as described in 3.1.3, the size of the incoming light does not affect the PSD output. The final distance between the PSD and the focus lens was 9 mm and the distance between the focus lens and the FSM 94 mm. Simulations show, that the entire active area and regions around it is irradiated by the laser. The resulting image is shown in Figure 3.19. The entire active area of the PSD has been mapped.

Due to the larger laser spot, the PSD is still partially and weakly irradiated, while the majority of the spot is not on the active area anymore. This leads to washed out borders and may result in inaccurate calculations. To minimize the washed out borders, a voltage threshold was defined, above which the beam is on the PSD. Rödiger et al. in [23] use a similar approach with their quadrant photo diode (QPD) sensor. They also define a voltage, under which the laser does not irradiate QPD and the resulting voltage is

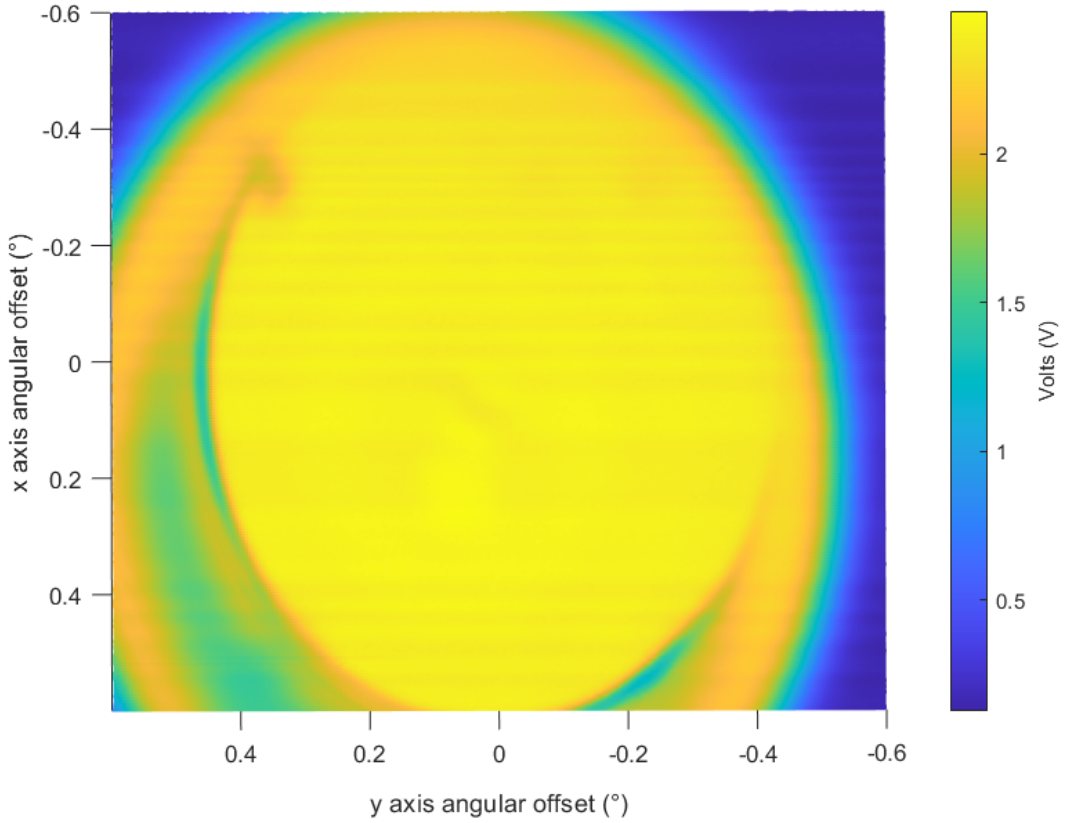

Figure 3.18 Sum of all quadrant voltages

considered noise due to environmental and hardware influences. The threshold for the PSD in the test track was chosen based on the voltage values of the four separate quadrants when the beam hits the edge of each quadrant. While the maximal sum of all voltages of all quadrants is 2.34 V according to Figure 3.19, each quadrant has a maximal value of 1.35 V, as shown in Figure 3.21. While after each spot, where the The final threshold value was 1.51 V and is larger than the maximal quadrant voltage, as the residual voltages of the other quadrants overlap and influence the sum. The resulting PSD area is shown in Figure 3.20.

Further investigation into the separate quadrants show the behavior that is expected, according to Sastry et al. [29]. Each quadrant returns their maximal value at the point furthest away from the center, as pictured in Figure 3.21. At that point, the laser is almost totally on the specific quadrant and therefore, the photocurrent is, proportional to the others, maximized. Yet it is important to see, that some residual photocurrents still flow through the other quadrants. This is because the PSD is an uninterrupted active surface. Therefore some current will always flow through each quadrant. Figure 3.21 also verifies that all four quadrants are symmetrical and the amplification of each channel has the same value. The basic functionality of the PSD is therefore verified.

Time Dependence

While Figure 3.20 and Figure 3.21 analyze the PSD in a spacial manner, it also needs to be analyzed in the time domain. The slew rate of $0.1°/s$ that was developed in Section 2.1.3 is relative slow. The PSD, therefore, does not need to be sampled at high rates in order to get accurate mirror movement data. However, since the test track is suppose to be used with future systems at the DLR, it is important to test its responsiveness. More importantly, it is of importance to check, if there is a time delay between the moving laser on the active surface and the voltage changes at the amplifiers. If the PSD outputs have a

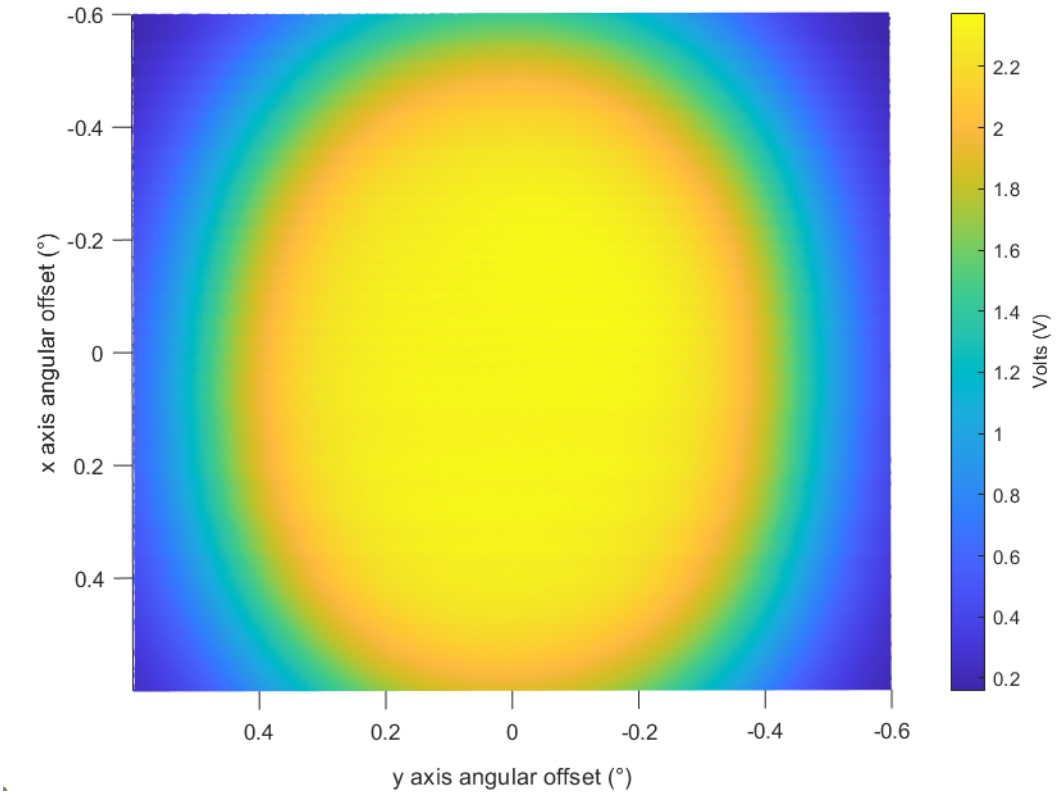

Figure 3.19 Sum of all quadrant voltages after distance reduction

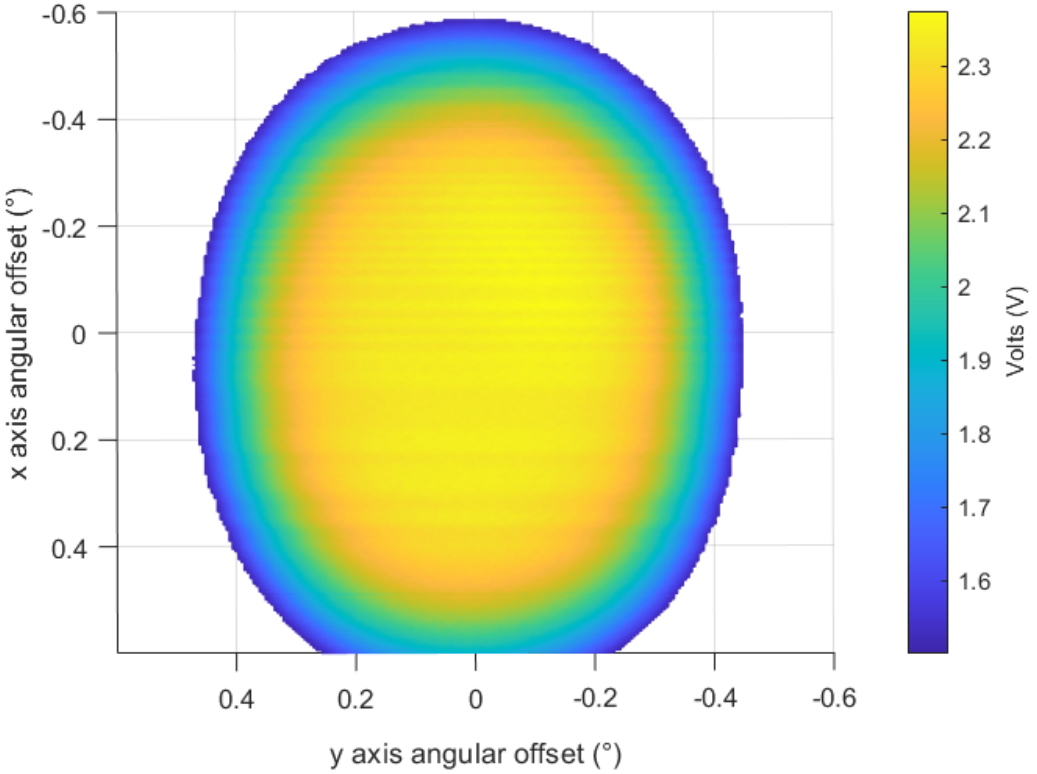

Figure 3.20 Voltage distribution of each quadrant

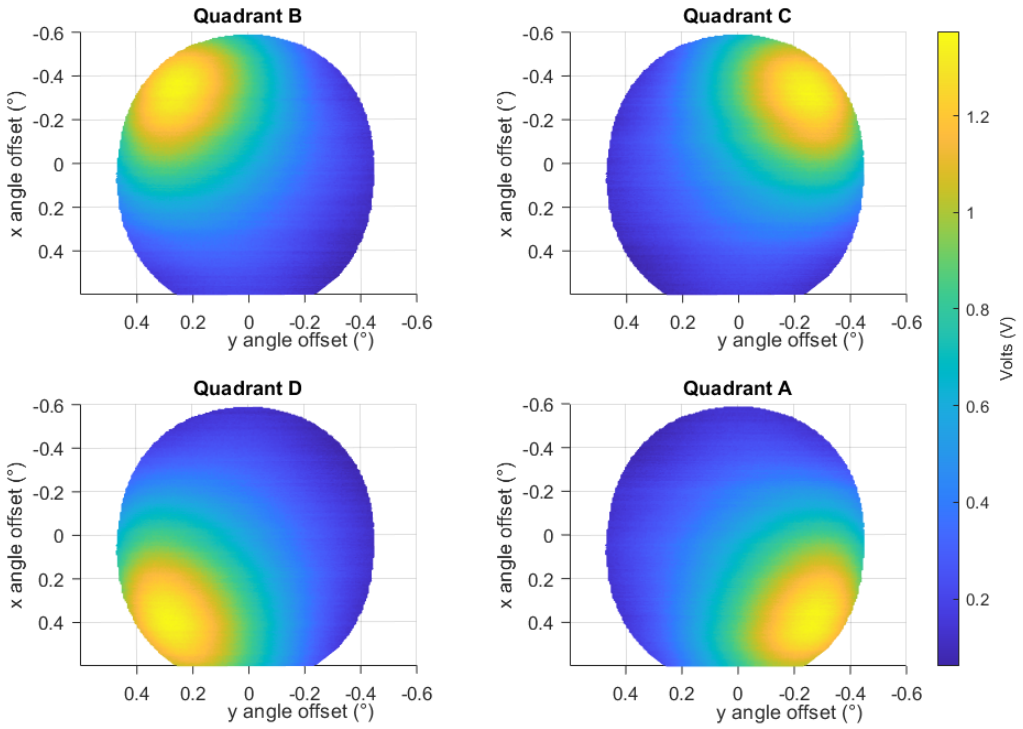

Figure 3.21 Voltage distribution of each quadrant

delay, then it needs to be evaluated, whether this delay renders the PSD unusable or whether it can be compensated through a time shift.

In order to test the responsiveness of the PSD, the DEMCON mirror was moved from $0° \rightarrow -0.6°$ in the x axis direction, while y stayed constant at zero. With this step, the step response of the PSD was recorded and compared to the regulated angular offsets of the DEMCON FSM. During the tests, the PSD and DEMCON FSM are sampled with a 20 kHz frequency, in order to record their behavior in great detail.

Figure 3.22 shows the step response of the quadrant B. The uninterrupted orange line is the step command send from the speedgoat to the FSM. The dotted-dashed line is the actual angular movement of the FSM in the x axis and the dashed line the movement of the y axis. The DEMCON FSM needs 25 ms to reach the $-0.6°$ offset after the set command has been send. This is consistent with the properties in the data sheet. The voltages from quadrant B follow the movement without delay.

Figure 3.23 shows an overview of all quadrants and their step response to the DEMCON FSM movement. All quadrants point to the same behavior. They react immediately to the changing laser position. The top two quadrants decrease in voltage, while the bottom two increase in voltage. This is due to their arrangement from Figure 3.4. By moving the laser spot from the center to the bottom half of the PSD, the photocurrent through the top two quadrants decrease while the bottom photocurrents increase.

This test validates the time dependence of the PSD. It proves that the PSD reacts immediately to change. Therefore this system can be used not only for the slower compact CPA tests, but also for future applications at the DLR.

Linearity

Lateral-effect diodes, like the one used in this setup, generally ensure a good linearity. The higher the quality, the greater the linearity is. In the real world, most units exhibit linearity within 0.5 percent over the central 25 percent of their active area, within 3 percent out to 75 percent of area and within 25 percent out to the periphery of the sensor [29].

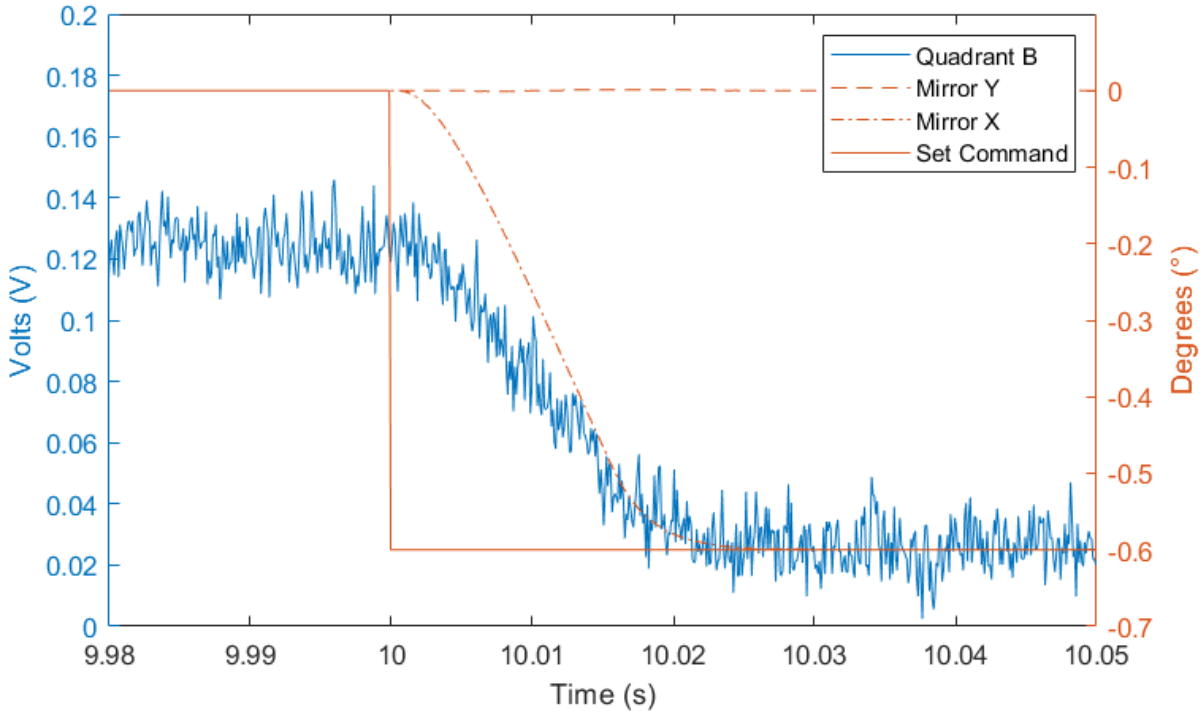

Figure 3.22 Step response of quadrant B after an FMS movement from $0° \rightarrow -0.6°$

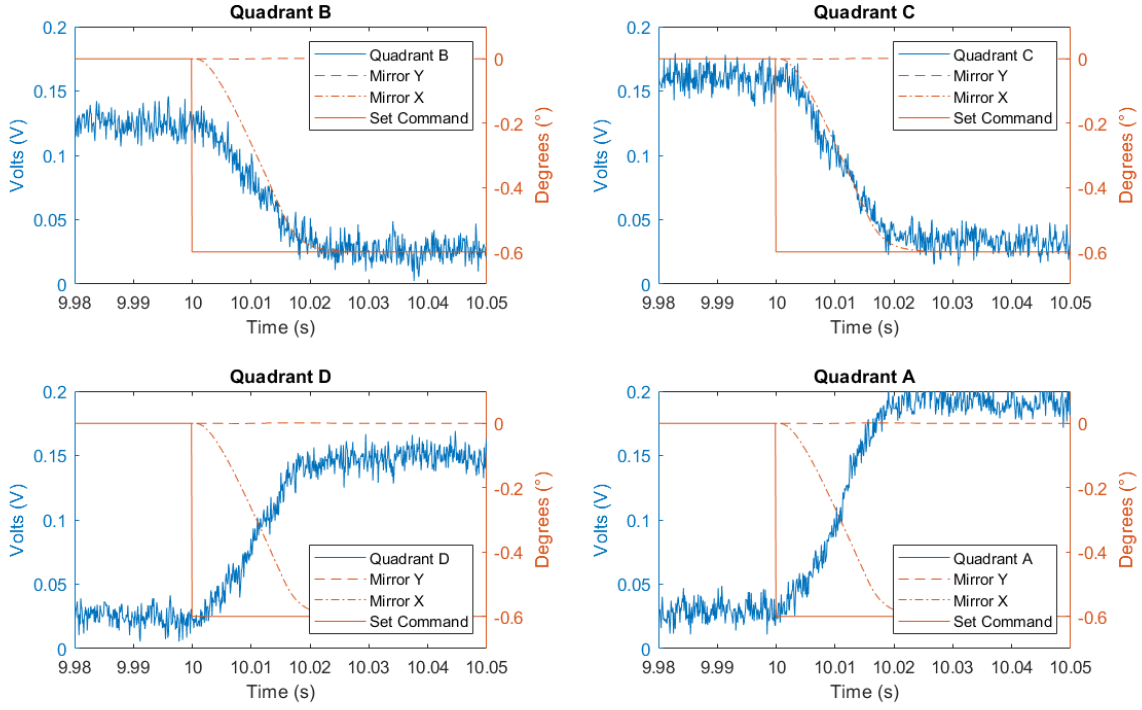

Figure 3.23 Step response of all quadrant after an FMS movement from $0° \rightarrow -0.6°$

The linearity of the sensor is important for accurate position calculations. Without constant linearity, the laser position can not be correctly estimated and without the exact position of the laser, the angular offset cannot be calculated. As a result, the the tests would lead to unusable data and the inability to characterize the mirror under test.

The linearity of the PSD can be calculated by using the horizontal and vertical differences of the quadrants. From the four quadrants the horizontal and vertical differences are calculated with equations 3.14 and 3.15 respectively.

$$T_{horiz} = \frac{(B+D)-(A+C)}{A+B+C+D} \tag{3.14}$$

$$T_{vert} = \frac{(B+C)-(A+D)}{A+B+C+D} \tag{3.15}$$

For the horizontal calculation, the PSD is split into two half circles consisting of quadrant B and D and quadrant A and C. The sums of the voltages of each half circle is subtracted and divided by the sum of all quadrants. This equation is applicable at each point on the PSD. The vertical calculations are performed with the half circles being orientated vertically. The sum of quadrant A and D are subtracted from the sum of quadrant B and C. Equation 3.14 and 3.15 lead to a normalized distribution of the voltages across the entire PSD.

Figure 3.24 shows the horizontal and vertical voltage distributions for the PSD mapping from Figure 3.20. At first glance, the distributions look as predicted. The constant, uniform slope that represents the linearity. At the edges, however, the constant, uniform slope starts to become nonlinear. In Figure 3.24a, the extreme cases on the vertical axis form two bulges at the edges of the circle. This is visible through the brighter yellow and darker blue tones. The same behavior can be examined in Figure 3.24b. There, at the extreme ends of the horizontal axis two bulges are present as well. However, this irregularity in the linearity can occur in the last 25 percent of the PSD area, as stated by [29].

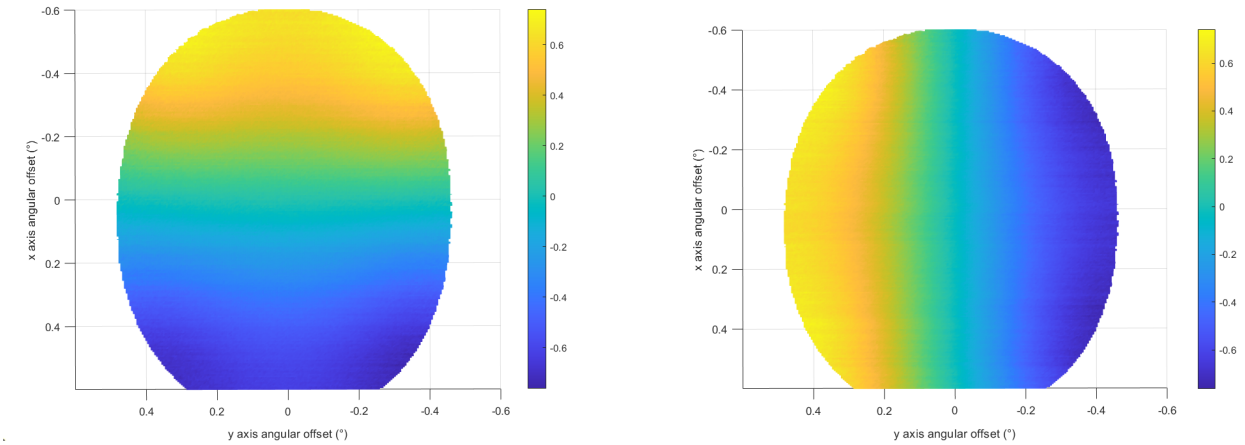

(a) Horizontal voltage distribution

(b) Vertical voltage distribution

Figure 3.24 Normalized voltage distributions of entire PSD area

Position Calculation

The relative voltages of the PSD readouts from equation 3.14 and 3.15 need to be converted to absolute position values. For these calculations, T_{horiz} and T_{vert} are multiplied with half the diameter of the active PSD area. D_{PSD} is 2.5 mm. The resulting equations for the x and y position are Equations 3.16 and 3.17, respectively.

$$x = T_{horiz} * \frac{D_{PSD}}{2} \tag{3.16}$$

$$y = T_{vert} * \frac{D_{PSD}}{2} \tag{3.17}$$

For each voltage combination of the four quadrants, a corresponding position can be calculated. To test the equations and the voltage distributions T_{horiz} and T_{vert}, specific patterns were driven with the DEMCON FSM. These were half circles of different diameters that crossed two quadrants of the PSD. The diameter of the half circle was the angular offset of the DEMCON FSM. Three different radii were chosen based upon the angular offsets from Figure 3.20. One at the very center of the PSD area, one further out, and one at its edge; $0.1°$, $0.2°$, and $0.3°$, respectively. The half circle with the radius of $0.3°$ in the relation to the coordinate system of the DEMCON FSM is pictured in Figure 3.25.

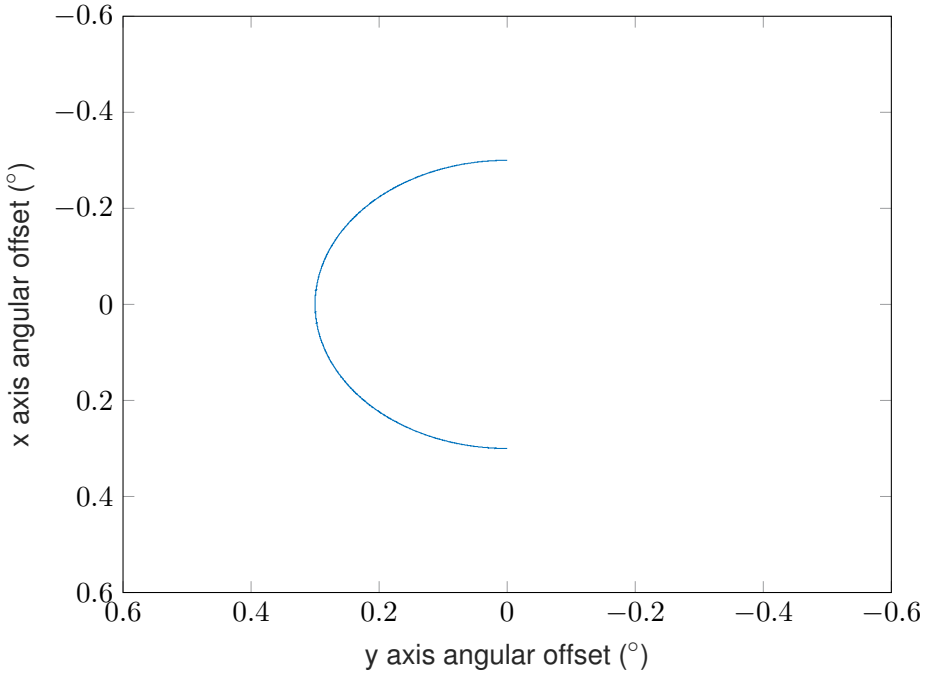

Figure 3.25 Voltages of the amplified photocurrents of all PSD quadrants without an active laser

Using the voltage distributions T_{horiz} and T_{vert} from the mapping of Figure 3.20, the position values for all three circles were calculated. These are shown in Figure 3.26. The circle with the $0.1°$ radius in Figure 3.26a is resembling the original movement from the FSM. The circle with the $0.2°$ radius in Figure 3.26b is plotted most accurately, while the circle with the $0.3°$ radius in Figure 3.26c shows serious deformations at its edges. Some magnitude of deformation from the $0.3°$ circle was expected, since it is placed at the edges of the active area of the PSD, where the linearity strongly decreases. Even with the expected deformations, the position calculations did not work. All three circles have the same radius. This cannot be correct. Furthermore, this wrong radius is very close to the radius of the PSD, meaning that each circle is in the nonlinear region of the PSD. Especially the $0.1°$ movement of the DEMCON FSM hits the PSD very close to the center. A radius of 2.3 mm is much larger than the expected value of 0.8 mm.

The reason for this incorrect position data must lie in the linearity of the PSD. To further investigate the linearity behavior, the position data was calculated over the entire grid pattern used to map and align the PSD. Five different scenarios were evaluated in detail: the maximum movement for each of the four quadrants and one crossing over the center of the PSD. At each scenario, the laser passes vertically over the the PSD. Especially during the scenario that goes through the center, the linearity of the PSD should become visible.

The position values for the four quadrants are plotted in relation to the mirror offsets in Figure 3.27. It is clearly visible, that the areas at the edge of the PSD show a non-linear behavior. Especially around

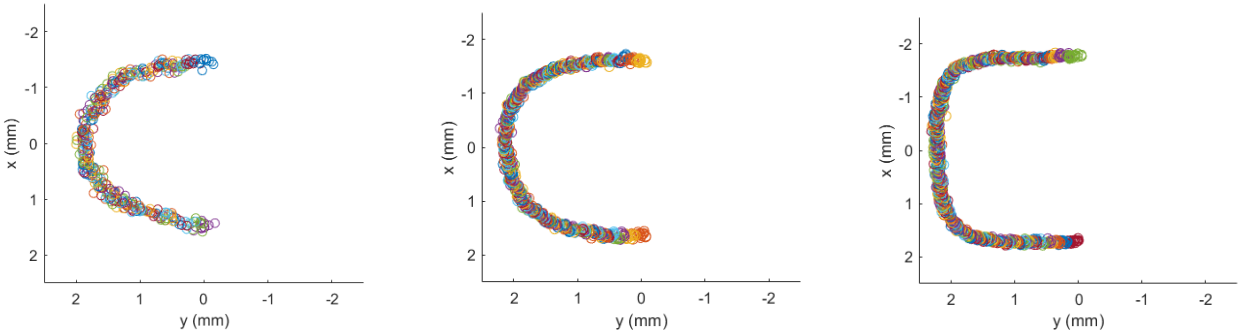

(a) Horizontal voltage distribution **(b)** Vertical voltage distribution **(c)** Vertical voltage distribution

Figure 3.26 Normalized voltage distributions of entire PSD area

the angular offsets of $\pm 0.5°$. However, this behavior is expected. The edges of the PSD are never linear. Although the y positions should not move, they are very volatile; even in the linear section of the sensor. This is evident in all subplots of Figure 3.27. The purple line moves considerably, when the y angular offset of the FSM goes though zero. If the x angular offset is drawn into consideration, it also becomes clear that these points are located near the edge of the PSD.

The fifth scenario focuses on the center of the PSD. According to [29], the PSD should behave linearly in this area. Figure 3.28 shows the opposite. Again, at the maximum angular y axis offsets non-linear behavior can be observed. The x position calculation are approximately linear in the range $\pm 0.2°$. The y position, however, is not linear in this range.

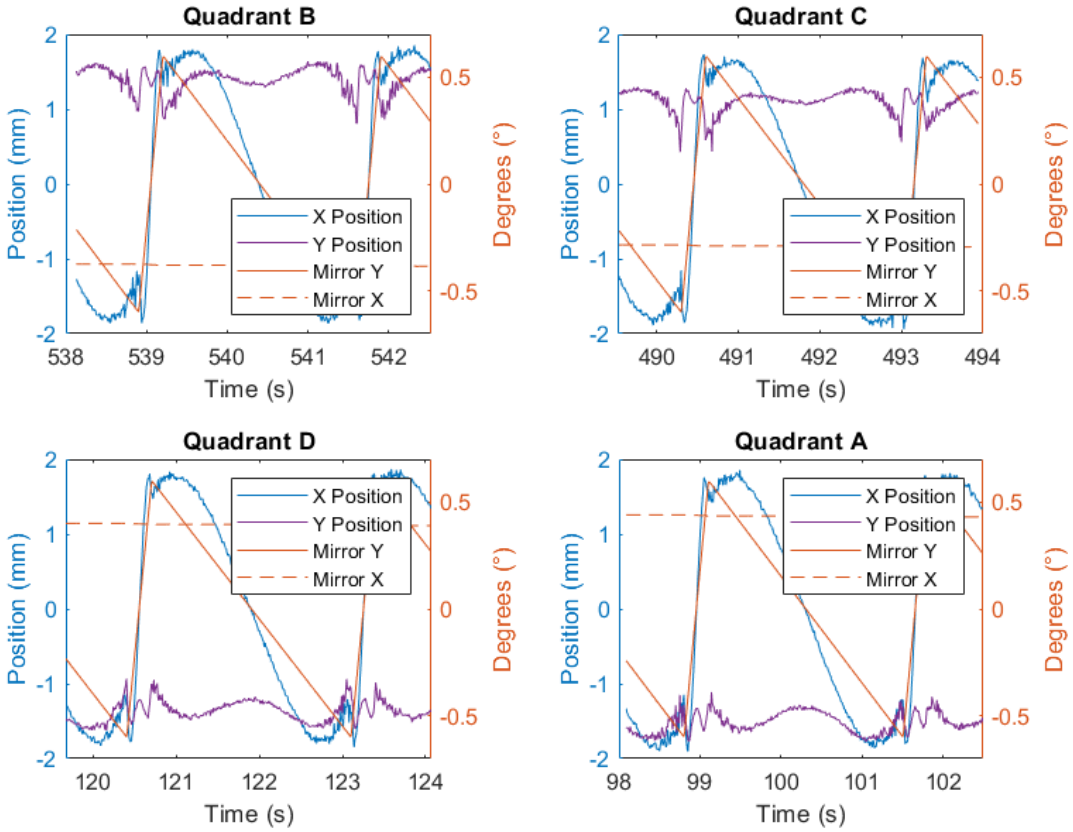

Figure 3.27 Position values of each maximal movement in each quadrant

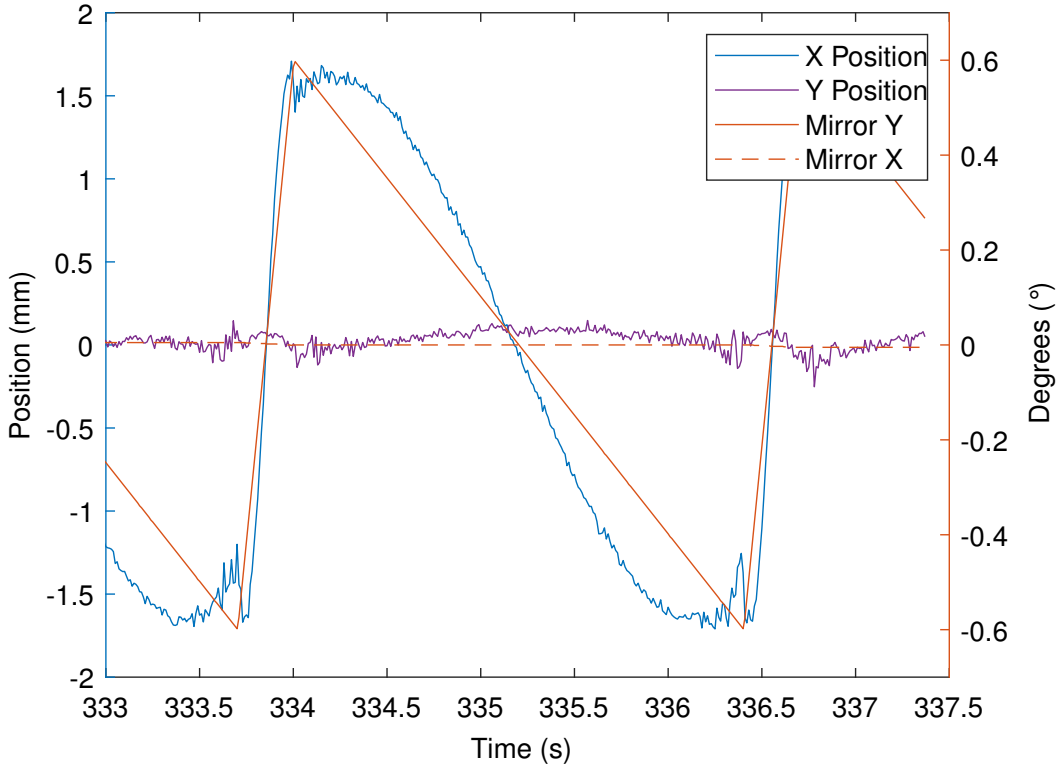

Figure 3.28 Position values of the movement trough the center of the PSD

PSD Conclusion

The linearity issues of the PSD cause laser spot position calculations to be inaccurate. Without these values, it is not possible to calculate the angular mirror offset. As a result, this PSD cannot be used for the characterization of mirror systems.

In order to make the test track fully operational, the PSD needs to be exchanged. The ISL Terminal uses a 4-Quadrant Diode (4QD) to acquire the beacon and measure the angular offset. Even though a 4QD has free spaces between its quadrants that lead to a worse resolution at these places, it works sufficiently to be used in a finalized system. A 4QD can be a valid replacement for the *IGA-050-PSD-E4* PSD, but due to time limitations and long delivery times no replacement for the PSD could be acquired during this thesis.

3.5.2 Test Track

Even though the PSD is not suited for precise position calculation, it could still be used to verify the functionality of the $4f$-Relay. The main goal is to verify equations 3.6, 3.7, and 3.8 and that larger angles of incidence still land on the PSD. At first, the DEMCON FSM was used to verify equations 3.6, 3.7, and 3.8. Then, the larger range of motion of the Optotune mirror was used to test the bigger angles of incidence.

Figure 3.29a shows the step response of quadrant B with a $0° \rightarrow -0.6°$ jump. It is the same step response as in Section 3.5.1. Since the laser moves downwards on the PSD, it moves away from quadrant B. Therefore, the voltage decreases. Once the $4f$-Relay is installed into the test track, the same step is driven on the DEMCON FSM. The results are shown in Figure 3.29b. The DEMCON FSM still moves downwards, but the voltage of quadrant B increases. This means, that the laser must be moving upwards, or, the movement is being mirrored. The decreaseed starting voltage of Figure 3.29b comes from the added optical elements of the $4f$-Relay. Through this experiment, equations 3.6 and 3.8 are verified.

In order to verify the $4f$-Relay with larger angles, the DEMCON FSM was replaced with the Optotune mirror. The mirror holder from Figure 3.12c and Figure 3.12d were installed to properly align the mirror

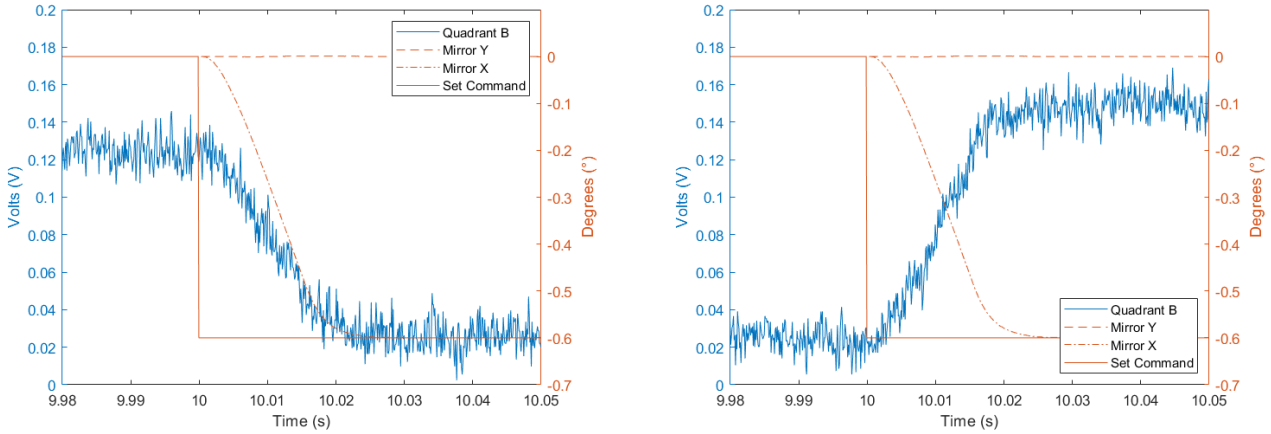

(a) Without $4f$-Relay

(b) With $4f$-Relay

Figure 3.29 Step response of quadrant B without $4f$-Relay (left) and with $4f$-Relay (right)

with the optical axis of the test track. The first tests were performed with a 600 nm, visible red laser. By deflecting the Optotune mirror, the resulting spot was visually inspected at the focus lens. The spot radiated onto an installed sight disk, which visualized the laser's movement. The angular movement of the mirror were mirrored at the focus lens.

The rudimentary test, investigated the angular offsets, that could be compensated by the $4f$-Relay, while staying in the CA of the lenses. The mirror movements simulated in Figure 3.10 did not clip the lens edges and stayed within their CA.

Further tests were not possible, since the software *Optotune Cockpit*, which controls the Optotune mirror, ran into irreversible problems. Restarts of all systems, re-installation of the software, and contact with Optotune's Tech-Support could not solve the encountered problems.

$4f$-Relay Conclusion

The rudimentary functionality of the $4f$-Relay could be verified through step responses with the DEMCON FSM and through large mirror deflections of the Optotune mirror. However, a detailed investigation of the limitations of the $4f$-Relay still need to be undertaken. As a result, the $4f$-Relay can be used to increase the distance between the mirror and the PSD while retaining the angle of deflection.

4 Newson Mirror System Commissioning

Due to the delayed delivery of the Newson Mirror System, the planned tests could no longer be carried out. To simplify the commissioning of the mirror in the future, this chapter summarizes the steps that need to be undertaken.

Basic Connectivity and First Tests

Connect the NMS to the master control unit and test the basic functionality of the mirror system. Then mount the NMS into the test track and repeat some basic movements. Analyze the PSD values.

NMS Characterization

The maximal angular movements, its linearity throughout the movement range, the step and frequency response, and the drift are all important factors of the NMS, which need to be explored during in-depth tests.

Thermal Tests

Once the NMS has been characterized, the environmental test follow. First, the thermal behavior is analyzed. The mirror is operated for a longer period of time and the thermal progression of the actuator is measured. The need for a heat sink must be evaluated and possible movements which do not create excessive thermal energy should be developed.

When the thermal behavior under an atmosphere is well understood, the same tests need to be repeated in an vacuum chamber. This is to test its cooling ability through radiation.

Vibration Test

The vibration tests serve two purposes. First, the resonance frequency of the NMS must be found out. Then, the internal feedback loop and the robustness of the coil mechanism are tested by submitting the system to vibrations of various frequencies and amplitudes. Shock resistance is also tested, in order to verify the accepted launch forces.

Radiation Testing

After all important test have been successfully completed, the NMS can be tested for its radiation resistance. This test must be conducted last, since permanent damage can be caused to the electronics. A decision must be made whether to irradiate the NMS with the expected LEO radiation or to irradiate it with the maximum accepted energy until the system breaks.

Depending on the results of these test, radiation shielding must be taken into consideration for the CubeSat design.

CubeSat Integration

The compact CPA needs to be developed further by building a prototype. This prototype must also be tested for its resonance frequency, as well as, its thermal behavior in a vacuum.

Once these test have been successfully completed, the compact CPA can be connected to an ISL Terminal. The control loop from the hemispherical CPA needs to be adjusted to the limitations of the NMS and the pin connections of the compact CPA need to be routed through the data handling unit of the ISL Terminal.

Finally, the combined communication system 'ISL Terminal — compact CPA' needs to be verified. This is done by shining lasers from different angles onto the subsystem to simulate the irradiation in space.

5 Integration into CubeSat

The design of the 1U CubeSat compact CPA is dependent on the configuration of the satellite it is integrated into. Due to its purpose as an inter-satellite link, two compact CPAs are needed to be able to communicate with the leading and trailing satellites in one orbit. Each CPA is coupled with an ISL Terminal. Therefore, 4U are needed to enable a continuous inter-satellite link without the necessity of body pointing. This limits the possible CubeSat sizes, on which this system can be integrated. Since more cubes are needed for a functioning satellite (power supply/body pointing/etc.), only the 6U and 12U units come into question. The arrangement of CubeSat units in 6U and 12U satellites is shown in Figure 5.1a and 5.1b, respectively.

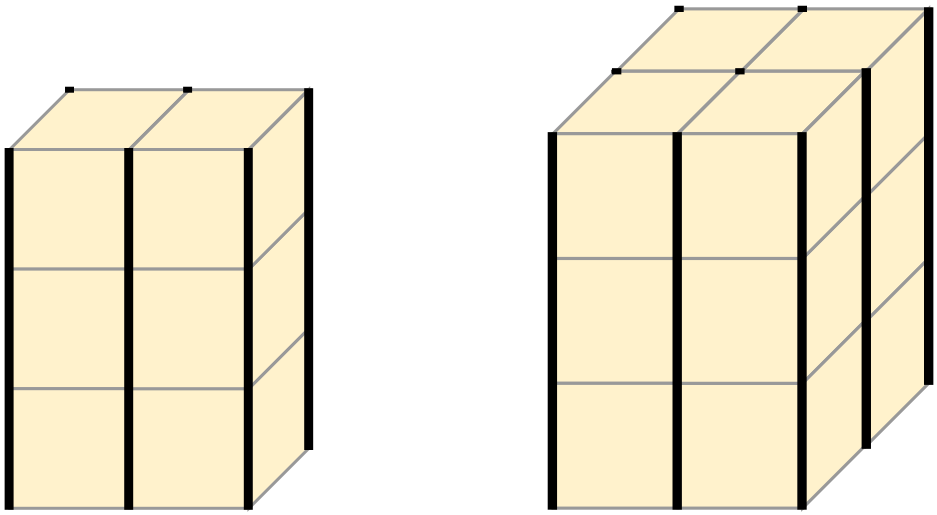

(a) Vertically orientated 6U CubeSat

(b) Vertically orientated 12U CubeSat

Figure 5.1 Possible CubeSat sizes for continuous inter-satellite communication with two ISL Terminals and compact CPAs

5.1 Preliminary Designs

The compact CPA is only integrated into a CubeSat coupled with the ISL Terminal. Therefore, the design of the compact CPA Unit is dependent on the structure of the ISL Terminal. The ISL Terminal design of Figure 2.1 shows that the optical axis of the telescope is vertical to the axis of the CubeSat rails. These rails are fixed elements and cannot be changed. They provide a standardized structure to which a unit's fixtures are connected to and act as a uniform system to easily connect multiple units together.

The NMS within the compact CPA needs to be aligned with the optical axis of the ISL Terminal's telescope. And due to the vertical rails in the ISL Terminal and the placement of the telescope, the CPA needs to be placed adjacent to it, to be correctly aligned, as the block diagram of Figure 5.2 shows. Figure 5.3 depicts the two coupled units in relation to CubeSat rails. Furthermore, the position of the telescope is not centered within the 1U unit; it is offset to the left side. This shift limits the position of the NMS within the compact CPA.

In the block diagram of Figure 5.2, the basic functionality of the two units coupled together is illustrated. The incoming laser beam is redirected onto the telescope while the outgoing beam is directed towards

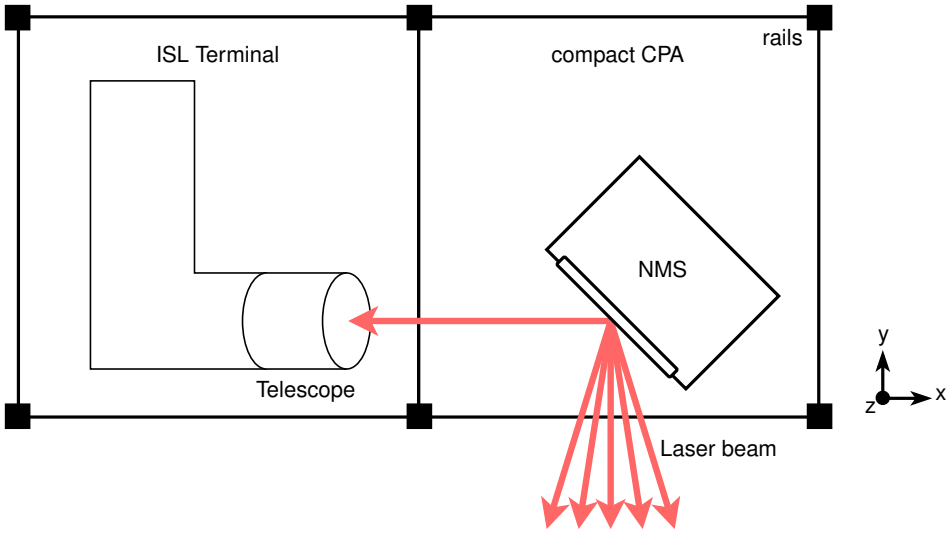

Figure 5.2 Block diagram of ISL Terminal coupled to compact CPA (not to scale)

the next satellite. The shift of the telescope determines the placement of the NMS. It limits the degrees of movement in the y and z axes, as otherwise the aperture would no longer be irradiated. As a result, the NMS can only be adjusted in the x direction and can only be rotated around the x axis. The 60 mm diameter of the NMS limits the lateral movement further since the housing may not be outside the 10 x 10 x 10 cm cube.

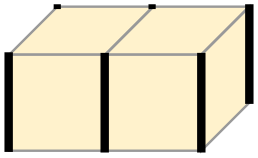

Figure 5.3 ISL Terminal and compact CPA cube arrangement

The center of the telescope is only 25.8 mm away from the edge of the 1U cube. Due to its 60 mm diameter, the NMS cannot be rotated around the x axis for multiple compact CPA variations, which are illustrated by the possible laser beam directions in Figure 5.4. The rotated NMS's housing would be outside the defined cube. The laser beam can also not enter and exit the CPA from the same axis as the telescope (purple arrow in Figure 5.4). The angle of incidence θ onto the NMS would be so large, that due to the relationship

$$d_{beam} = d_{mirror} * \sin(\theta) \tag{5.1}$$

the redirected beam would not fully irradiate the 20 mm aperture of the telescope anymore. Adding a fixed mirror into the compact CPA and moving the NMS, as shown in Figure 5.5 is also not a feasible option. While the laser beam can be reflected at a smaller angle of incidence and therefore the entire

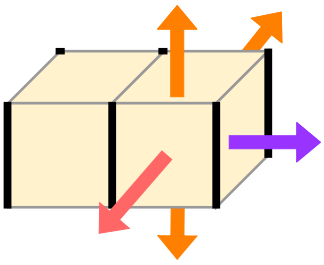

Figure 5.4 Feasible laser beam direction (red) and non feasible laser beam directions (orange & purple) due to NMS rotation within compact CPA unit

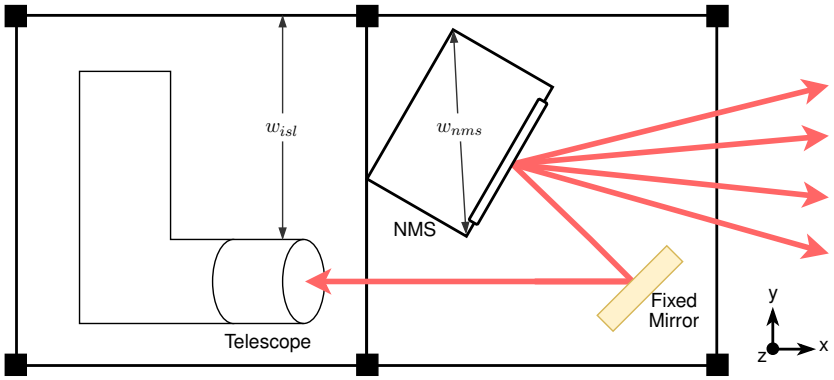

Figure 5.5 Block diagram of the theoretical beam path, if the laser enters CPA at the front (not to scale)

20 mm aperture of the telescope could be irradiated, the width w_{isl} of 52 mm is too small to fit the diagonal NMS length w_{nms} of 73 mm. The reflected beam of the fixed mirror would be clipped by the NMS and not hit the telescope completely.

As a result, the orientation of the NMS from the block diagram in Figure 5.2 and the corresponding red arrow in Figure 5.4 is the only possible option for accommodating the NMS in the 1U. While this makes it possible to optimize this one variation of the compact CPA, it greatly limits the options for various CubeSat installation configurations. The different installation configurations and the resulting satellite orientations are discussed in Section 5.2.

The resulting compact CPA from the block diagram in Figure 5.2 is shown in Figure 5.6. There, only one wall segment is attached to the 1U cube, since this connects to the heat sink of the NMS. The wall provides the surface area for the thermal energy to radiate into space. Since this is only a preliminary design and a full thermal simulation of the finalized compact CPA was not undertaken, it is not quite certain whether this connection and the extra radiating surface is needed. If future tests show that the NMS stays within its designed thermal window without this cooling mechanism, it could be removed. All outside surfaces, except the one where the laser beam enters and exits the cube, can be built freely by the satellite manufacturer. Either further CubeSat units or the outer cladding of the satellite can be attached.

The opening, where the laser beam enters and exits the cube, does not require a glass pane. Normally, glass would protect the inside optical components from environmental hazards like humidity, dust, and rain. In space, however, all these types of threats are not existent. It would rather become an obstacle. First, the glass would need to be treated with AR coatings to minimize reflections. The refraction through the glass pane would need to be taken into consideration and the extra mass would increase the launch cost, while also increasing the unit cost. Significantly, the glass pane would not protect the NMS from the space environment. It does not act as shielding for ionized particles, nor can it reduce the impact of the space vacuum, the magnetic fields, and the incoming solar rays. The damage by small space debris or meteorites is not reduced by a thin glass pane. On the contrary, the pane may even aggravate the impact of such an object. While a small object, a screw for example, could miss the NMS and would only hit the housing, a pane would shatter upon impact and the whole CPA would be rendered useless because of cracks in the pane. Therefore, it was decided not to add a glass pane at one side of the compact CPA CubeSat unit.

5.1.1 Electronics Integration

The modulation and power electronics for the NMS also need to be incorporated into the 1U unit. The PCB from Figure 3.13a was redesigned in order to have one board controlling both channels, rather than stacking the original PCB. The new board was adapted to the CubeSat PCB standards. This makes the integration easier since it can be connected directly to the frame. The multiple Molex connectors on the ISL Terminal also mean that the larger SMA connectors can be replaced with smaller and lighter Molex

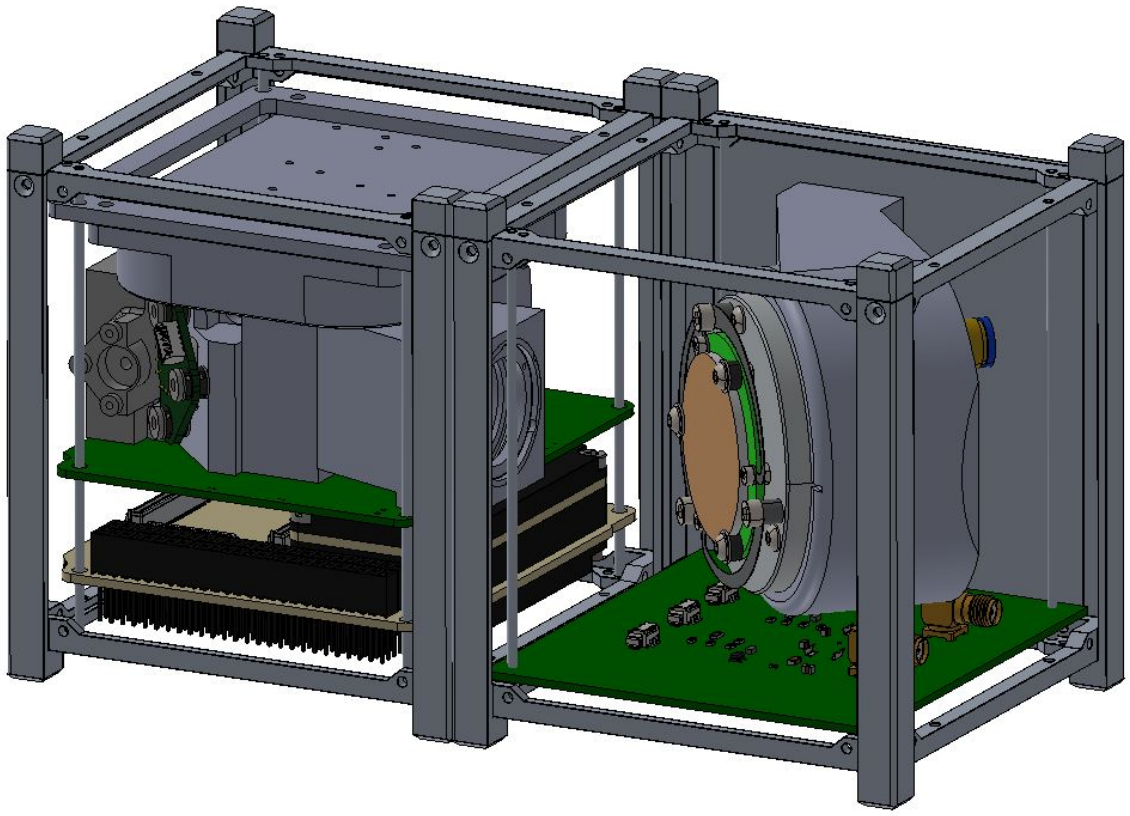

Figure 5.6 Preliminary design of the compact CPA coupled to the ISL Terminal

connectors. This reduces the PCB footprint even further. Only two SMA connectors are needed to connect to the NMS. They cannot be replaced with any other connector. The final design is shown in Figure 5.7.

The actual positioning of the PCB within the 1U offers a lot of freedom. As long as the PCB does not block the laser beam, it can be positioned anywhere. To minimize mass and complexity, it is desired to minimize the required cable length to the ISL Terminal ports and to the NMS. Therefore it is best placed close to the data handling unit of the ISL Terminal, as done in Figure 5.6. There, the distance from the SMA connectors at the top of the PCB to the NMS is the shortest, while the distance from the Molex connectors on the other side to the adjacent ISL Terminal is also minimized. The cables need to be secured to the housing to minimize the possibility of them moving. Movement could be caused through vibrations and shocks. Over the duration of the mission, such emerging movements can put stress on the connectors, induce components collision, or loosen the cable connection, which could ultimately lead to a disconnection of the cables. That would be a catastrophic failure since the compact CPA would become uncontrollable and the satellite could not continue its mission objectives. Therefore, larger components and cables are generally fully adhered to the housing or adjacent mounted components with glue. The placement on the edge of the cube also aids in thermal management, since the electronics power dissipation can be radiated to the space environment more easily.

5.2 Integration into CubeSat

The compact CPA always needs to be facing to the direction towards the leading or trailing satellite. Since the ISL Terminal and CPA subsystem must always be installed in a specific constellation, it limits the installation options in a CubeSat, but also the possible satellite orientations in space. Figure 5.8 shows an example of two 6U CubeSats and their necessary orientation in order to be able to communicate with the leading or trailing satellite on their perspective orbital path. The red arrows resemble the in- and outgoing laser beams.

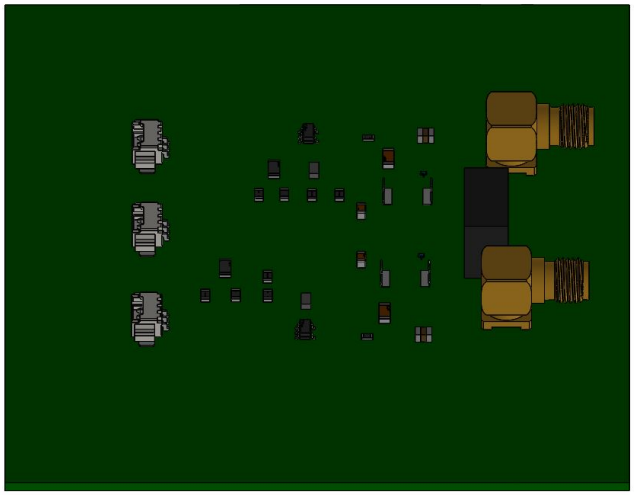

Figure 5.7 Final NMS modulation and power electronics PCB

The ISL Terminal and compact CPA subsystem do not need to be placed at the top and bottom rows of a CubeSat. Their placement can be determined freely and in such a way that the overall layout of all satellite modules is optimized. The functionality of the CPA is not affected, if it is rotated $180°$ around its x axis, relative to the coordinate system from Figure 5.2. This means, that the arrows in Figure 5.8 can come from both cubes in one row on the same side. The rotation around the x axis does not have an effect on the communication link. The large distance between the satellites means that the partner satellite is completely irradiated due to the propagating laser beam. Therefore, the position of the CPA within the satellite does not affect its communication abilities. The rotation around the x axis of the subsystem would only have an effect on the integration with the other satellite modules. The satellite manufacturer would decide, in which orientation the ISL Terminal and compact CPA subsystem is most effective in respect to the entire satellite.

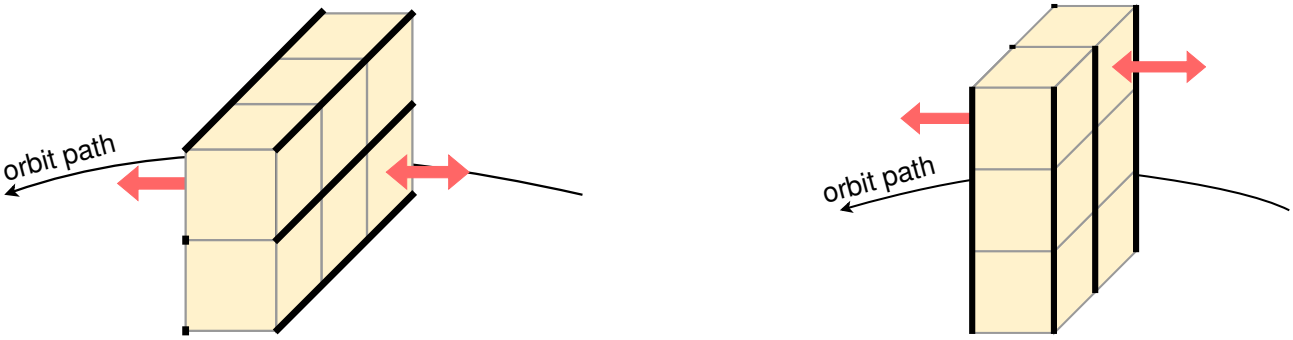

(a) Horizontally orientated 6U CubeSat

(b) Vertically orientated 6U CubeSat

Figure 5.8 CubeSat orientation and CPA communication direction relative to orbital path

5.3 Commissioning

Before a system is launched into space, considerations must be made about the forces it will be subject to during launch. Dependent on the launch vehicle and the orientation of the satellite in relation to the launch vehicle, considerable forces may be exerted onto certain parts. If these parts are not designed to withstand such forces, they could be damaged during the launch. To prevent this from occurring, these components can be locked in place with a Launch Lock. A Launch Lock prevents unwanted motion and secures the thus controlled components. Current Launch Locks are based on pyrotechnic, electro-mechanically or

NiTi driven pin pullers and they are mostly one time use mechanisms that are usually bulky and involve a relatively high mass [2]. The use of such a system would safeguard the functionality of the NMS but would add further complexity, mass, and points of failure. The necessity of a launch lock therefore needs to be carefully evaluated based on each launch vehicle.

Each satellite's system must be tested and calibrated as soon as the satellite reaches its final orbit; this also includes the compact CPA. It must be ensured that the launch did not impair the mirror and its electronics. A predefined procedure was developed in order to ensure the functionality of the system.

1. The NMS is powered up and the system awaits a response from the NMS. If this happens, all components are still connected, the mirror is responsive and the PCB has not suffered any damage from the launch.

2. To calibrate the NMS, a bright object is needed from which one knows the exact position in relation to the satellite. This can be the moon, a planet, or a bright star. The sun is not a good alternative, since direct irradiation of all sensors with the full power of the sunlight can cause damage.

   By using the satellite's body pointing, one CPA of the satellite is angled towards the bright space body. Then the acquisition concept for the ISL Terminal, developed by Rödiger et al. [23], is executed to center the bright object onto the quadrant photo diode in the ISL Terminal. Once completed, the angular offset of the mirrors is used to calculate the actual direction of the bright body in respect to the satellite's position. These values are then compared with the theoretical values that are based on the satellite's orientation, its GPS position, and space object's location in relation to the satellite. The difference of the theoretical and practical value is the NMS offset. This offset can then always be included in the calculation.

3. The above procedure must be run twice. Once while the satellite is being irradiated by the sun and once while the orbit is in the shadow of the Earth. This ensures functionality in both temperature ranges; the offset must be the same in both cases. If not, it must be compensated accordingly.

This is just a rough draft and needs to be developed in much more detail. The development of a detailed commissioning procedure is not part of this thesis, as the complexity of this topic would go beyond its scope.

6 Conclusion

The goal of this paper —the development of a stand-alone mirror system that can be attached to a pre-existing communication terminal to increase its range of operation— was achieved. A comprehensive requirements list was developed, which encompasses every aspect of the mirror actuator. The requirements list is based on current LEO constellations, specific requirements from the DLR and its partners, and from the physical space environment.

After thorough research and discussions with multiple companies, a suitable mirror actuator was chosen that meets most technical requirements. The Mirror System *Cyclops* from the Belgian company Newson is the final choice. The combination of a large reflective surface of 38.1 mm and an angular movement range of 240 mrad, not only offers sufficient mirror movement for the planned missions with the ISL Terminal, but also makes the compact CPA suitable for a large variety of future projects. This makes the NMS extremely flexible in its operational application and allows it to be considered beyond the compact CPA in other communication terminals, like ground stations or for intermediate CPA in planes.

In order to test the chosen NMS, a test track was developed. The test track's purpose is to provide a controllable and stable environment, in which a mounted mirror system can be characterized and the effect of various environmental factors can be tested. The test track is divided into four subsystems: a laser collimator, the mirror under test, a PSD, and a $4f$-Relay. Each of these components were tested separately to ensure the overall functionality of the test track.

During the functionality tests of the test track, it became clear that the PSD is not suited for the use in this setup. This was caused by the non-linearity of the sensor which leads to inaccurate position calculations and therefore inaccurate mirror movement calculations. On a test track that is designed to analyze the movement of a mirror system, the position calculations and the subsequent angle calculations of the PSD are of upmost importance.

The test track has been extended so that future mirror systems can be tested as well. An additional FSM can be integrated into the optical path to introduce vibrations and disturbances. The mirror under test must be able to compensate these disturbances. As a result, the control speed and accuracy can be tested.

The preliminary designs of the compact CPA show that the incoming laser can successfully be redirected to the ISL Terminal and the angular movement range compensates for any angular misalignments. The power draw of the entire system is so low, that it can be used continuously to ensure a stable connection between two satellites and furthermore, the modulation of the signal is carried out on its own PCB so that the PCB of the ISL Terminal does not have to be unnecessarily loaded.

The compact CPA upholds the technical CubeSat requirements from [6] and can therefore be defined as an 1U CubeSat unit. The standardized platform simplifies the integration with the ISL Terminal and the integration into the entire satellite, also providing sufficient flexibility to be configured effectively by the space craft designer.

6.1 Future Plans

The PSD of the test track needs to be replaced with a model, which exhibits better linearity. The new PSD then needs to be thoroughly tested and integrated into the setup.

Due to the global supply chain disruptions that have affected every industry after COVID-19, the delays in the delivery of the Newson Mirror System meant that many planned test could not be carried out. These test are of high importance during the validation process of a component for satellites. Without these tests and their results, the behavior of the mirror actuator cannot be characterized sufficiently and its resistance to the space environment cannot be reliably evaluated.

Therefore, once the NMS is delivered to the DLR institute, further characterization work must be carried out and the environmental tests conducted. The thermal behavior in vacuum is of high importance to ensure functionality in space, as well as the radiation tests to ensure the NMS can withstand the space environment.

Once the NMS is integrated into the 1U CubeSat, the resonance frequency of the entire compact CPA must be determined in order to avoid standing oscillations and possible interference with other satellite units. The thermal behavior of the entire CubeSat unit needs to be simulated and tested in a vacuum chamber to ensure the thermal energy of the electronics can be radiated into space, while the Albedo Effect and the direct radiation of the sun do not heat up the compact CPA excessively.

Finally, the commissioning protocol of Section 5.3 must be further developed to guarantee a successful commissioning and operation of the compact CPA once the CubeSat has reached its final orbit.

A Newson Mirror System

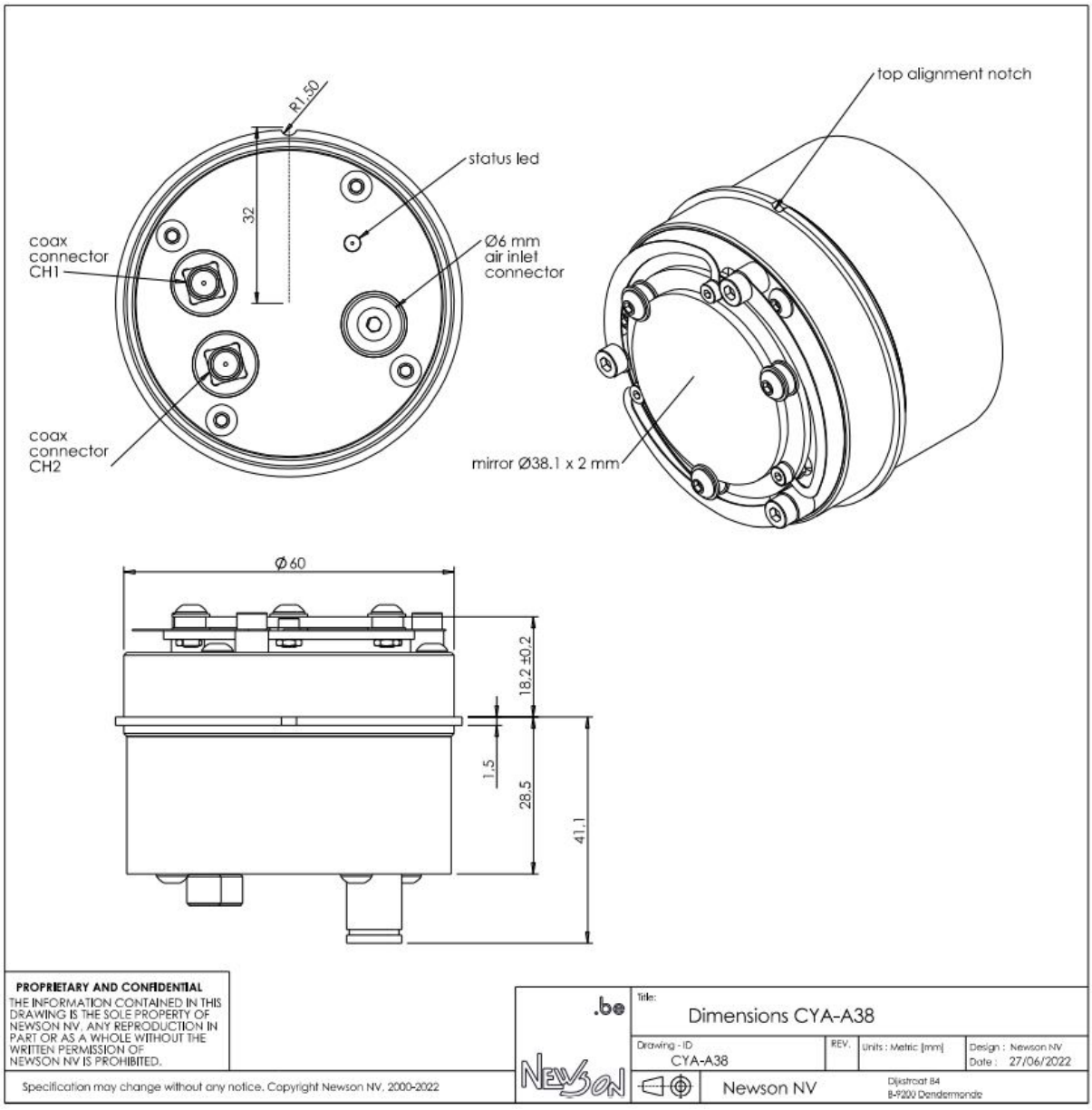

Figure A.1 Newson Mirror System Dimensions

B THORLABS Complete Bill of Materials

Name	Thorlabs Article Number	Quantity
Aluminium Breadboard	MB3030/M	1
Post Holder with Hex-Locking Thumbscrew, L = 40 mm, Vacuum Compatible	PH40V/M	4
Post Holder with Hex-Locking Thumbscrew, L = 50 mm, Vacuum Compatible	PH40V/M	1
Vacuum-Compatible Optical Post, M4 Setscrew, M6 Tap, L = 40 mm	TR40V/M	3
Vacuum-Compatible Optical Post, M4 Setscrew, M6 Tap, L = 50 mm	TR50V/M	2
Cage Assembly Rod, 8" Long, Ø6 mm	ER8	8
Cage Assembly Rod, 1" Long, Ø6 mm	ER1	2
Cage Assembly Rod, 1.5" Long, Ø6 mm	ER1.5	2
30 mm Cage Plate with Ø1" Double Bore, M4 Tap	CP35/M	1
Snap-On 60 mm Cage Mounting Bracket, M4 Tap	LCPMA2/M	2
30 mm to 60 mm Cage Plate Adapter, M4 Tap	LCP33/M	3
30 mm to 30 mm Cage System Right-Angle Adapter	CP30	1
60 mm to 30 mm Cage System Right-Angle Adapter	LCP30	1
60 mm Cage System Translating Lens Mount for Ø2" Optics	CXY2	1
Kinematic 30 mm-Cage-Compatible Mount for Ø1" Optic	KC1/M	1
Right-Angle Kinematic Mirror Mount, 30 mm Cage System and SM1 Compatible	KCB1C/M	1
Ø1" Unthreaded Adapter for Ø11 mm Cylindrical Components	AD11NT	1
SM1 to M9 x 0.5 Lens Cell Adapter	S1TM09	1
SM1 to M12 x 0.5 Lens Cell Adapter	S1TM12	1
1550 nm, f = 15.58 mm, NA = 0.16 FC/PC Fiber Collimation Pkg.	F260FC-1550	1
f=7.5 mm, Ø5 mm Achromatic Doublet, M9x0.5 Threaded Mount	AC050-008-C-ML	1
f=10 mm, Ø8 mm Achromatic Doublet, M12x0.5 Threaded Mount	AC080-010-C-ML	1
f=35 mm, Ø1" Achromatic Doublet, SM1-Threaded Mount	AC254-035-C-ML	2
ADD SILVER MIRROR		1

Bibliography

[1] Optotune AG. Fov and clipping calculation sheet. Excel Sheet, 2016.

[2] Mircea Badescu, Xiaoqi Bao, and Yoseph Bar-Cohen. Shape memory alloy (sma)-based launch lock. volume 9061, page 90613L, 04 2014.

[3] Aaron C. Boley and Michael Byers. Satellite mega-constellations create risks in low earth orbit, the atmosphere and on earth. *Nature Sci Rep*, 11(10642), 2021.

[4] Max Born and Emil Wolf. *Principles of optics*. Cambridge University Press, Cambridge, England, 7 edition, 1999.

[5] Carlos Carrizo, Markus Knapek, Joachim Horwath, Dionisio Diaz Gonzalez, and Paul Cornwell. Optical inter-satellite link terminals for next generation satellite constellations. In Hamid Hemmati and Don M. Boroson, editors, *Free-Space Laser Communications XXXII*, volume 11272, page 1127203. International Society for Optics and Photonics, SPIE, 2020.

[6] The CubeSat Program, Cal Poly SLO. *CubeSat Design Specification (1U - 12U)*, July 2020. Rev. 14.

[7] M Detaille. Hard gold coating. In *Submillimetre and Far-Infrared Space Instrumentation*, volume 388, page 73, 1996.

[8] DLR. Communication, navigation and quantum technology. https://www.dlr.de/content/en/articles/space/communication-navigation-and-quantum-technology.html, October 2022.

[9] DLR. Dlr at a glance. https://www.dlr.de/EN/organisation-dlr/dlr/dlr-at-a-glance.html, October 2022.

[10] DLR. A pioneering launch – compact satellite pixl-1 carries the world's smallest laser terminal into orbit. https://www.dlr.de/content/en/articles/news/2021/01/20210124_pioneering-launch-compact-satellite-with-smallest-laser-terminal.html, October 2022.

[11] Yukio Fukui, Tsunehiro Takeda, and Takeo Iida. Systematic generation method of relay optical systems. *Appl. Opt.*, 29(13):1947–1951, May 1990.

[12] MRC Systems GmbH. Laser-strahlstabilisierung. https://www.mrc-systems.de/de/produkte/laser-strahlstabilisierung, September 2022.

[13] F Graham Smith, Terry A King, and Dan Wilkins. *Optics and Photonics*. Wiley-Blackwell, Hoboken, NJ, 2 edition, apr 2007.

[14] Eugene Hecht. *Optik*. de Gruyter Studium. de Gruyter, 7 edition, mar 2018.

[15] Gregory Hollows and Nicholas James. Understanding focal length and field of view. https://www.edmundoptics.com/knowledge-center/application-notes/imaging/understanding-focal-length-and-field-of-view/, June 2022.

[16] Edmund Optics Inc. Effects of laser mirror surface flatness. https://www.edmundoptics.com/knowledge-center/application-notes/optics/effects-of-laser-mirror-surface-flatness/, October 2022.

[17] Wilfried Ley, Klaus Wittmann, and Willi Hallmann. *Handbuch der Raumfahrttechnik*. Carl Hanser Verlag GmbH & Co. KG, München, 5 edition, 2019.

[18] Newson NV. *'CYCLOPS' SINGLE MIRROR DEFLECTION SYSTEMS*, July 2022. Rev. 2.0.

[19] Newson NV. Cyclops. http://newson.be/cyclops.htm, October 2022.

[20] Optotune AG. *Dual axis mirror with position feedback MR-15-30*, May 2022. Rev. 1.1.

[21] Optotune AG. *MR-E-2 Development Kit Operation Manual*, March 2022. Rev. 1.0.

[22] Dr. Ruediger Paschotta. Fiber collimators, Jun 2022.

[23] Benjamin Rödiger, Rene Rüddenklau, Christopher Schmidt, and Marc Lehmann. Acquisition concept for inter-satellite communication terminals on cubesats. In *Small Satellites Systems and Services - The 4S*, May 2022.

[24] Benjamin Rödiger, Christian Fuchs, Jorge Rosano Nonay, Wolfgang Jung, and Christopher Schmidt. Miniaturized optical intersatellite communication terminal – cubeisl. In *2021 IEEE International Conference on Communications Workshops (ICC Workshops)*, pages 1–5, 2021.

[25] SmarAct. Stt-2013 - tip-tilt-mirror mount. https://www.smaract.com/en/opto-mechanics/product/stt-2013, September 2022.

[26] THORLABS. Fast steering mirror. https://www.thorlabs.de/catalogPages/622.pdf, September 2022.

[27] THORLABS. Qs30xy-ag. https://www.thorlabs.de/thorproduct.cfm?partnumber=QS30XY-AG, September 2022.

[28] THORLABS. Superior off axis performance. https://www.thorlabs.com/newgrouppage9.cfm?objectgroup_id=4066&pn=AC254-035-C-ML, September 2022.

[29] United Detector Technology. *Using Photodetectors for Position Sensing*, 12 1988.

[30] University of Surrey. *Blue Sky Thinking on Computer Networks in Space*, 39 BB 02, Department of Computer Science, Alan Turing Building, Stag Hill Campus, University of Surrey, Guildford, jul 2022. Nishanth Sastry and Jonathan Black and Mohammed Kassem.

[31] Han Woong Yoo, David Brunner, Thomas Thurner, and Georg Schitter. Mems test bench and its uncertainty analysis for evaluation of mems mirrors. *IFAC-PapersOnLine*, 52(15):49–54, 2019. 8th IFAC Symposium on Mechatronic Systems MECHATRONICS 2019.